

## QUASARS PROBING QUASARS VII. THE PINNACLE OF THE COOL CIRCUMGALACTIC MEDIUM SURROUNDS MASSIVE $Z \sim 2$ GALAXIES

J. XAVIER PROCHASKA<sup>1,2</sup>, MARIE WINGYEE LAU<sup>1</sup>, JOSEPH F. HENNAWI<sup>2</sup>

*Draft version June 21, 2018*

### ABSTRACT

We survey the incidence and absorption strength of the metal-line transitions C II 1334 and C IV 1548 from the circumgalactic medium (CGM) surrounding  $z \sim 2$  quasars, which act as signposts for massive dark matter halos  $M_{\text{halo}} \approx 10^{12.5} M_{\odot}$ . On scales of the virial radius ( $r_{\text{vir}} \approx 160$  kpc), we measure a high covering fraction  $f_C = 0.73 \pm 0.10$  to strong C II 1334 absorption (rest equivalent width  $W_{1334} \geq 0.2 \text{ \AA}$ ), implying a massive reservoir of cool ( $T \sim 10^4$  K) metal enriched gas. We conservatively estimate a metal mass exceeding  $10^8 M_{\odot}$ . We propose these metals trace enrichment of the incipient intragroup/intracluster medium that these halos eventually inhabit. This cool CGM around quasars is the pinnacle amongst galaxies observed at all epochs, as regards covering fraction and average equivalent width of H I Ly $\alpha$  and low-ion metal absorption. We argue that the properties of this cool CGM primarily reflect the halo mass, and that other factors such as feedback, star-formation rate, and accretion from the intergalactic medium are secondary. We further estimate, that the CGM of massive,  $z \sim 2$  galaxies accounts for the majority of strong Mg II absorption along random quasar sightlines. Lastly, we detect an excess of strong C IV 1548 absorption ( $W_{1548} \geq 0.3 \text{ \AA}$ ) over random incidence to 1 Mpc physical impact parameter and measure the quasar-C IV cross-correlation function:  $\xi_{\text{CIV-Q}}(r) = (r/r_0)^{-\gamma}$  with  $r_0 = 7.5^{+2.8}_{-1.4} h^{-1}$  Mpc and  $\gamma = 1.7^{+0.1}_{-0.2}$ . Consistent with previous work on larger scales, we infer that this highly ionized C IV gas traces massive ( $10^{12} M_{\odot}$ ) halos.

*Subject headings:* absorption lines – intergalactic medium – Lyman limit systems

### 1. INTRODUCTION

The detection of a strong emission feature at 7 keV from the hot plasma surrounding the Perseus cluster revealed that its intracluster medium (ICM) is enriched in heavy elements (Mitchell et al. 1976). This marked the discovery that gas within dark matter halos was enriched over the past 13 Gyr. Modern X-ray experiments have extended the measurements to clusters at  $z \gtrsim 1$  and have recorded metallicities of  $\approx 1/3$  solar across this  $\approx 10$  Gyr time period (e.g. Baldi et al. 2012; Andreon 2012). If one extrapolates these data to the virial radius, the total metal mass is extraordinary –  $4 \times 10^{10} M_{\odot}$  in Fe alone (e.g. Sivanandam et al. 2009) – and offers a challenging constraint to models of chemical enrichment (e.g. Zaritsky et al. 2004; Bonaparte et al. 2013). The tension is sufficiently strong that researchers continue to debate/discuss whether one must invoke non-standard initial mass functions (IMFs) and/or stellar yields for galaxies in cluster environments (e.g. Portinari et al. 2004; Arrigoni et al. 2010; Loewenstein 2013; Yates 2014). Recently, the latest generation of X-ray telescopes have extended such studies to lower mass systems ( $M \approx 10^{13} M_{\odot}$ ;  $kT \sim 1$  keV). These ‘groups’ also exhibit a highly enriched medium to at least  $r_{\text{vir}}/2$ , with a mass in Fe alone that exceeds  $10^9 M_{\odot}$  (Sasaki et al. 2014).

Despite the ongoing arguments over the IMF and yields, these enrichment models all agree that the gas that forms the ICM must have been polluted at early

times, when massive galaxies form the majority of their stars. In the models of Portinari et al. (2004), for example, over 50% of the Fe and O is injected into the ICM after only a few Gyr. With early enrichment of the ICM a uniform prediction, one is well motivated to search for direct evidence of this activity. The cleanest signature might be the observation of a large mass in metals in the proximity of massive high- $z$  galaxies, far beyond the stars that drive the enrichment. Gas in this environment is commonly referred to as halo gas or the circumgalactic medium (CGM). Unfortunately, such an experiment cannot be carried out through X-ray emission because of surface brightness dimming, the likelihood that the gas is too cool, and the redshifting of the putative emission to energies  $\lesssim 2$  keV. And while deep H I Ly $\alpha$  imaging has proven successful in discovering diffuse and extended emission around galaxies (e.g. Matsuda et al. 2004; Cantalupo et al. 2014), metals from such nebulae are rarely detected. Furthermore, estimating the gas metallicity and metal mass would be very challenging (Arrigoni-Battaia et al. 2014).

For these reasons, one is compelled to perform the search in absorption using background sources whose sightlines pass close to massive, high- $z$  galaxies. This experiment is also difficult to perform, in particular to discover and characterize high- $z$  galaxies that lie foreground to sufficiently bright, background sources. Steidel and collaborators have spent 100+ nights on the 10m Keck telescopes to perform their Keck Baryonic Structure Survey (KBSS; Adelberger et al. 2005b; Steidel et al. 2010; Rakic et al. 2012) which focuses on the star-forming, Lyman break galaxies (LBGs) at  $z \sim 2$ . Analysis of the observed clustering of LBGs, however, implies dark matter halo masses  $M_{\text{halo}} \lesssim 10^{12} M_{\odot}$  (Adelberger et al. 2005b;

<sup>1</sup> Department of Astronomy and Astrophysics, UCO/Lick Observatory, University of California, 1156 High Street, Santa Cruz, CA 95064

<sup>2</sup> Max-Planck-Institut für Astronomie, Königstuhl 17, D-69115 Heidelberg, Germany

Bielby et al. 2013). While relatively massive, the majority of LBGs are not predicted to evolve into the massive galaxies representative of clusters and massive groups (Conroy et al. 2008). Furthermore, despite the tremendous observational investment, the sample of quasar sightlines probing the galactic halos of LBGs remains modest ( $\sim 10$ ; Rudie et al. 2012; Turner et al. 2014) and other groups have provided only a few additional cases (Cooke et al. 2006; Simcoe et al. 2006; Crighton et al. 2011). Nevertheless, the results to date do indicate a halo of enriched, cool gas traced extending to an impact parameter  $R_{\perp} \approx 100$  kpc. Crighton et al. (2013) has studied one sightline in great detail, finding a low metallicity for the less ionized material and a near solar metallicity for a more highly ionized phase. Ongoing analysis will examine similar properties for the full sample to characterize (with large sample variance) the enrichment of this halo gas.

For studying ICM enrichment, one would preferably perform a similar experiment with a large sample of more massive galaxies, i.e.  $M_{\text{halo}} > 10^{12} M_{\odot}$  at  $z = 2$ . This is a primary goal of our Quasar Probing Quasars<sup>3</sup> (QPQ) survey. Over the past decade, we have discovered a large sample of close quasar pairs through a dedicated, follow-up effort on candidates drawn from the SDSS, BOSS, and 2dF surveys and confirmed with spectroscopy from 4m-class telescopes including: the 3.5m telescope at Apache Point Observatory (APO), the Mayall 4m telescope at Kitt Peak National Observatory (KPNO), the Multiple Mirror 6.5m Telescope, and the Calar Alto Observatory (CAHA) 3.5m telescope (Hennawi 2004; Hennawi et al. 2006b, 2010; Bovy et al. 2011, 2012). A large fraction of the confirmed pairs are physically unassociated, i.e. the quasars have distinct redshifts indicating that they lie at cosmologically large separations. With this sample of projected pairs, we recognized that one could explore the CGM of massive galaxies at  $z \sim 2$  using the f/g quasars as “signposts”. Assuming that the scaling relations between massive black holes and galaxies holds at this epoch, these active nuclei tag massive galaxies in the young universe. Indeed, the galaxy masses inferred from the measured clustering of quasars yields estimates for the dark matter halos  $M_{\text{halo}} \approx 10^{12.5} M_{\odot}$  (White et al. 2012; Vikas et al. 2013). In this manner, we established the QPQ survey, a dedicated analysis of the properties of gas surrounding quasars on scales of a few tens kpc to  $\sim 1$  Mpc. This probes gas on scales within the virial radius of massive galaxies ( $r_{\text{vir}}^{\text{QPQ}} \approx 160$  kpc) and beyond. One predicts that the galaxies hosting quasars evolve into the massive dark matter halos associated to groups and clusters in the modern universe ( $M > 10^{14} M_{\odot}$ ; Fanidakis et al. 2013). In these respects, the QPQ experiment addresses the enrichment and heating of the incipient ICM and intragroup medium (IGrM).

Thus far, the QPQ survey has focused primarily on H I Ly $\alpha$  absorption. We recognized in our first analyses (QPQ1, QPQ2: Hennawi et al. 2006a; Hennawi & Prochaska 2007) that the incidence of H I optically thick absorbers (aka Lyman limit systems or LLS) about quasars was significantly higher than random, and measured a cross-correlation clustering ampli-

tude of  $r_0 = 9.2h^{-1}$  Mpc (Hennawi & Prochaska 2007). We then conducted a detailed study of the physical properties of one of these LLS (QPQ3: Prochaska & Hennawi 2009), finding a near solar metallicity, a significantly ionized medium, and extreme kinematics. In QPQ4 (Hennawi & Prochaska 2013), we searched sensitively for faint Ly $\alpha$  emission associated with these LLS and found no positive detections, implying that the low-ionization material frequently detected in our b/g sightlines is very likely shadowed from the quasar radiation by the same obscuring medium invoked in unified models of AGN (e.g. Antonucci 1993). The most recent publications studied further the CGM via H I Ly $\alpha$  absorption (QPQ5, QPQ6: Prochaska et al. 2013b,a). We confirmed the high incidence of optically thick gas, with an excess above the random incidence to at least 1 Mpc (physical). Similarly, the data exhibit excess H I Ly $\alpha$  absorption on all scales within 1 Mpc in the transverse direction, with a stronger signal than complimentary measurements from any other galactic population. This follows from the fact that  $z \sim 2$  quasars are hosted by massive galaxies and, apparently, their radiative emission does not suppress cool gas absorption in the surrounding medium (transverse to the sightline). This large reservoir of H I runs contrary, however, to the predictions from zoom-in simulations of galaxy formation in massive dark matter halos even if one ignores quasar radiation (Fumagalli et al. 2014). This suggests that the models lack key aspects of the astrophysics that determine the properties of halo gas (see also QPQ6; Cantalupo et al. 2014).

It is possible that the presence of a quasar within these massive galaxies may complicate interpretation of the results. Wherever such luminous sources shine, they will over-ionize the medium to distances of  $\gg 100$  kpc (e.g., QPQ2; Chelouche et al. 2008). In H I Ly $\alpha$  absorption, one detects a line-of-sight proximity effect to distances of approximately 15 Mpc (Bajtlik et al. 1988; Scott et al. 2000). In the transverse direction, however, we and others have found little evidence for over-ionization; studies report the absence of a transverse proximity effect (TPE; Crofts 1989; Moller & Kjaergaard 1992; Croft 2004, QPQ6). We have concluded that quasars emit their ionizing radiation anisotropically (or on timescales of  $t \ll 10^5$  yr). In this manuscript, we proceed under the expectation that the quasar has little radiative impact on the majority of gas surrounding it. A major motivation of the QPQ survey, however, is to test this hypothesis and we search for evidence here of a significant transverse proximity effect.

We acknowledge that the presence of a luminous quasar undoubtedly represents a special epoch (likely repeated) in the life-cycle of massive galaxies. Even allowing for anisotropic emission, the number density of luminous quasars is at least an order of magnitude smaller than the number density of massive halos ( $> 10^{12} M_{\odot}$ ). Nevertheless, studies of the galaxies hosting quasars indicate that these systems have rather standard characteristics. Estimations of their star formation rate (SFRs) from sub-mm observations, for example, show that the galaxies in a quasar phase lie along the so-called ‘main sequence’ of star formation (Mainieri et al. 2011; Rosario et al. 2013). Searches for signatures that the quasar phase is triggered by an ongoing or recent galaxy-galaxy merger generally

<sup>3</sup> <http://www.qpqsurvey.org>

yield null results (e.g. Dunlop et al. 2003; Veilleux et al. 2009, but see also Canalizo et al. 2007; Bennert et al. 2008). Lastly, searches for CO emission from the galaxies hosting quasars do not find extreme gas masses nor unusual kinematics (Coppin et al. 2008; Simpson et al. 2012). The growing consensus is that quasar activity does not imply special conditions on galactic scales<sup>4</sup>.

This manuscript expands greatly on our study of metal-line absorption in the environments of  $z \sim 2$  massive galaxies, as first presented in QPQ3 and QPQ5. We focus primarily on the transitions of C II 1334 and the C IV  $\lambda\lambda 1548, 1550$  doublet, which are frequently observed in the ISM and IGM and whose larger rest-wavelengths often place them outside the Ly $\alpha$  forest. These ions also span a wide range of ionization conditions, probing gas that is predominantly neutral to highly ionized material. Our analysis presents an assessment of the gas enrichment to 1 Mpc, i.e. scales characteristics of the ICM/IGrM. These data also provide an assessment of the ionization state, albeit limited by the low-resolution of the spectra which preclude precise estimates of the column densities. An analysis of the smaller set of high-resolution spectra that provide ionic column density measurements will be the focus of a future work (QPQ8: Lau et al., in prep.).

Another motivation for studying the CGM of massive,  $z \sim 2$  galaxies is to explore the origin of halo gas in individual galaxies. Given the positive detections of enriched halo gas in the ICM and IGrM, it is reasonable to expect that the dark matter halos hosting individual galaxies like the Milky Way also contain a hot and enriched plasma. Unfortunately, this medium is either too cool or has too low mass to permit regular detection with X-rays, even using modern technology and techniques (e.g. Anderson et al. 2013). Instead, scientists have demonstrated that these lower mass halos do harbor a substantial reservoir of heavy elements by linking metal absorption systems discovered in quasar spectra to galaxy halos (Bergeron 1986). Initially traced by the Mg II doublet and now studied with other lines, this halo gas has a much lower temperature and ionization state than the hot ICM discovered in X-rays. This ‘cool CGM’ was first predicted by Bahcall & Spitzer (1969) and decades of absorption-line research have since statistically mapped the incidence and average surface density of ions ranging from Mg<sup>+</sup> to O<sup>+5</sup>, in galaxies large and small (e.g. Chen et al. 2010a; Prochaska et al. 2011; Tumlinson et al. 2011; Stocke et al. 2013; Werk et al. 2013). The growing consensus from these programs is that halo gas has a metal mass of at least  $10^7 M_\odot$  (Werk et al. 2014), exceeding the mass in metals of the ISM and possibly even that in stars (Peeples et al. 2013).

With the basic observables of the  $z \sim 0$ , metal-enriched CGM nearly well-defined, researchers are now striving to understand its origin and to resolve the physical phenomena that shape it across cosmic time. First and foremost, one requires a source of metals, i.e. stars, and we presume that these form and die primarily within galaxies (but see Zaritsky et al. 2004). Under this expectation, one must identify a mechanism to transport the

metals to large ( $> 100$  kpc) separations from the stellar systems. Theorists have proposed a variety of such processes, e.g., galactic scale winds, AGN feedback, cosmic ray pressure, tidal stripping. But while most of these have been ‘caught in the act’ driving gas/metals from galaxies (e.g. Veilleux et al. 2013; Ebeling et al. 2014; Rubin et al. 2013), their relative importance and impact over the lifetime of a galaxy are poorly constrained. In part, this results from the great difficulty in modeling such processes. The time-scales and large dynamic range required to capture the astrophysics of feedback remain an intractable computational problem, even in idealized simulations (e.g. Creasey et al. 2013). As such, numerical simulations inevitably resort to sub-grid prescriptions to model such processes. In this manuscript, we draw comparisons between the cool CGM of massive,  $z \sim 2$  galaxies and that for galactic populations with a diverse range of masses, ages, and SF histories. These comparisons offer insight into the origin and evolution of cool gas around galaxies.

This manuscript is summarized as follows. We present a summary of the data sample in Section 2 and the equivalent width measurements in Section 3. The primary observational results are given in Section 4 and these are discussed in Section 5. A summary and concluding remarks completes the main body of the manuscript (Section 6). An Appendix provides our own survey for strong C IV 1548 absorption in random sightlines and details on semi-empirical models for the cool, enriched gas surrounding LRGs. Throughout this manuscript, we adopt a  $\Lambda$ CDM cosmology with  $\Omega_M = 0.26$ ,  $\Omega_\Lambda = 0.74$ , and  $H_0 = 70 \text{ km s}^{-1} \text{ Mpc}^{-1}$ . When referring to comoving distances we include explicitly an  $h_{70}^{-1}$  term and follow modern convention of scaling to a Hubble constant of  $70 \text{ km s}^{-1} \text{ Mpc}^{-1}$ . All equivalent width measurements are presented in the rest-frame, unless otherwise specified.

## 2. DATA SAMPLE

The sample of quasar pairs analyzed here is a subset of the sample studied in QPQ6 for H I Ly $\alpha$  absorption. Specifically, we have restricted the current study to those pairs where the signal-to-noise (S/N) ratio at H I Ly $\alpha$  exceeds 9.5 per rest-frame  $\text{\AA}$ . This facilitates a more precise evaluation<sup>5</sup> of H I Ly $\alpha$  and generally insures sufficient S/N redward of Ly $\alpha$  for the metal-line analysis. Quasar emission redshifts are taken directly from QPQ6, following the methodology described in that manuscript. Briefly, we adopt a custom line-centering algorithm to centroid one or more far-UV emission lines and adopt the analysis of Shen et al. (2007) to combine these measurements and assess systematic uncertainty in the final value. The median emission redshift of the 427 pairs is  $z_{\text{em}}^{\text{median}} = 2.35$  and the median uncertainty in the redshift measurements is  $\approx 520 \text{ km s}^{-1}$ . The impact parameters range from  $R_\perp = 39 \text{ kpc}$  to 1 Mpc, with 52 pairs having  $R_\perp < 200 \text{ kpc}$ .

Generally, we have analyzed the same spectrum of the b/g quasar used to measure H I Ly $\alpha$ , as listed in Table 4 of QPQ6. The exceptions are primarily for data obtained with Keck/LRIS and Magellan/MIKE which employ dual cameras and a beam-splitting dichroic. For

<sup>4</sup> Note, however, that AGN discovered in galaxies selected for extreme properties (e.g. bright sub-mm emission; Wang et al. 2008) are obvious exceptions.

<sup>5</sup> In fact, this was the cutoff adopted in QPQ6 for the analysis of individual systems.

TABLE 1  
QPQ7 SPECTRA

b/g Quasar	f/g Quasar	$z_{\text{fg}}$	$R_{\perp}$ (kpc)	Instr.	$\lambda_r^a$ (Å)
J000216.66−053007.6	J000211.76−052908.4	2.8190	768	SDSS	1093-1738
J000432.76+005612.5	J000426.43+005703.5	2.8123	882	BOSS	1049-1638
J000531.32+000838.9	J000536.29+000922.7	2.5224	725	BOSS	1099-1747
J000633.35−001453.3	J000629.92−001559.1	2.3327	711	BOSS	1146-1638
J000838.30−005156.7	J000839.31−005336.7	2.6271	841	BOSS	1023-1715
J001025.73−005155.3	J001028.78−005155.7	2.4268	387	BOSS	1097-1728
J001634.35−010622.7	J001631.71−010426.9	3.5359	932	BOSS	834-1633
J001641.17+010045.2	J001637.10+005936.7	2.6690	760	BOSS	1044-1763
J002123.80−025210.9	J002126.10−025222.0	2.6912	299	BOSS	1059-1806
J002610.92−010213.0	J002613.63−010132.2	2.3260	491	BOSS	1178-2798
J002802.60−104936.0	J002801.18−104933.9	2.6591	175	Keck/ESI	1200-2756
J003138.17+003333.2	J003135.57+003421.2	2.2328	529	BOSS	1135-2826
J003423.40−104956.3	J003423.06−105002.0	1.8364	67	Keck/LRISb-1200/3400	1124-1365
				Keck/LRISr-1200/7500	1694-2084
				Keck/LRISr-600/10000	2331-3188
J003922.69+002642.9	J003924.54+002501.5	3.2980	819	BOSS	1068-1767
J004603.29+000729.4	J004600.47+000543.6	2.4526	960	BOSS	1066-1643
J004732.73+002111.3	J004738.19+001955.3	2.4826	940	BOSS	1031-2805
J010130.26+031822.0	J010134.93+031701.4	2.2718	912	BOSS	1097-2820
J010900.86+000137.1	J010857.21+000154.5	2.4169	486	BOSS	1147-2832
J011138.20+140414.9	J011144.06+140401.6	2.0019	749	Keck/LRISb-1200/3400	1038-1345
				Keck/LRISr-1200/7500	1564-1569
				Keck/LRISr-600/10000	2771-2848
J011149.39+140215.7	J011150.06+140141.3	2.4732	301	Keck/LRISb-1200/3400	950-1244
				Keck/LRISr-1200/7500	1548-1561
				Keck/LRISr-600/10000	2777-2834

NOTE. — [The complete version of this table is in the electronic edition of the Journal. The printed edition contains only a sample.]

<sup>a</sup> Rest-frame wavelengths at the f/g quasar redshift where the spectra of the b/g quasar exceeds  $S/N > 5$  per pixel.

those pairs, key metal-line transitions (e.g. the C IV doublet) tend to occur in spectra taken with the red camera. For MIKE, the spectral resolution and S/N of the data from the red camera are comparable to the data from the blue camera. For LRIS, we employed a number of gratings with the red camera. In approximately half of the pairs observed with Keck/LRIS we employed only the 300/7500 grating, which we consider too low of resolution to analyze metal-line transitions, or the wavelength coverage is uninformative with the chosen grating. We supplement the analysis of these pairs, when possible, with BOSS or SDSS spectra (Abazajian et al. 2009; Ahn et al. 2012).

For completeness, Table 1 lists all of the spectra analyzed in this study. In cases where multiple spectra covered the same transition, we gave preference to the higher spectral resolution unless the S/N was very poor. Details related to data reduction and calibration of the 1D spectra are provided in QPQ6. As a starting point, we employed the continua generated in QPQ6 for the H I analysis following standard principal component analysis (PCA) techniques (Lee et al. 2012, 2013).

### 3. EQUIVALENT WIDTH MEASUREMENTS

The heart of this analysis is the search for and measurement of metal-line transitions at  $z \approx z_{\text{fg}}$  in each quasar pair. Owing to the substantial uncertainty in quasar emission redshifts ( $\approx 500 \text{ km s}^{-1}$ ), we performed the search in  $3000 \text{ km s}^{-1}$  velocity windows centered on  $z_{\text{fg}}$ . The strongest transitions commonly detected in quasar spectra (e.g. Si II 1260, C II 1334, and the Si IV, C IV doublets) were explored first, restricting to spectral

regions outside the Ly $\alpha$  forest. This effort was first completed in support of the QPQ6 analysis, in particular to assist the assessment of whether the associated H I gas was optically thick. For this study, we have re-inspected all of the data and have performed new analysis as warranted.

In cases where one or more metal-line transitions were identified, we defined a narrower velocity region encompassing the absorption (typically  $100 - 200 \text{ km s}^{-1}$ ) for subsequent equivalent width measurements. As the default, one window was adopted for all metal-line transitions of a given quasar pair. In a small fraction of the cases, absorption from unrelated systems (typically Mg II or C IV doublets) lay coincident to the key transitions for the pair analysis. If the blending was modest, then these spectral regions were simply excluded in the equivalent width integrations. If the blending was severe, we excluded the transition from further analysis. If no strong absorption was evident in the search window for any of the metal-line transitions (corresponding to an  $\approx 3\sigma$  detection threshold), we adopted an analysis window roughly matching that used in the H I Ly $\alpha$  analysis of QPQ6 (see their Table 4). This generally corresponds to the absorption profile of the strongest Ly $\alpha$  line within the  $3000 \text{ km s}^{-1}$  window centered on  $z_{\text{fg}}$ . During the search, the local continuum was frequently adjusted to more accurately normalize the b/g quasar flux.

The equivalent width measurements  $W_{\lambda}$  were derived from simple boxcar integrations within the analysis regions and uncertainties were estimated from standard error propagation using the  $1\sigma$  uncertainties in the normalized flux. These do not include uncertainties related to

TABLE 2  
QPQ7 EW MEASUREMENTS

f/g Quasar	b/g Quasar	$R_{\perp}$ (kpc)	$z_{\text{fg}}$	$\delta v^a$	$W_{1334}$ (Å)	$\sigma(W_{1334})$ (Å)	$W_{1548}$ (Å)	$\sigma(W_{1548})$ (Å)
J000211.76–052908.4	J000216.66–053007.6	768	2.819	-232	0.001	0.035	0.044	0.066
J000426.43+005703.5	J000432.76+005612.5	882	2.812	-429	0.051	0.132		
J000536.29+000922.7	J000531.32+000838.9	725	2.522	317	0.160	0.084	0.113	0.262
J000629.92–001559.1	J000633.35–001453.3	711	2.333	40			0.084	0.268
J000839.31–005336.7	J000838.30–005156.7	841	2.627	551	0.069	0.054		
J001028.78–005155.7	J001025.73–005155.3	387	2.427	-797			0.049	0.136
J001631.71–010426.9	J001634.35–010622.7	932	3.536	578	-0.048	0.144	0.089	0.094
J001637.10+005936.7	J001641.17+010045.2	760	2.669	-925			0.368	0.113
J002126.10–025222.0	J002123.80–025210.9	299	2.691	841			0.351	0.282
J002613.63–010132.2	J002610.92–010213.0	491	2.326	-239			1.956	0.140

NOTE. — [The complete version of this table is in the electronic edition of the Journal. The printed edition contains only a sample.]

<sup>a</sup> Velocity offset from  $z_{\text{Ly}\alpha}$  to  $z_{\text{fg}}$ . Note that absorption lines were assessed only for data with  $S/N_{\text{Ly}\alpha} > 9.5$ .

continuum placement, which contribute  $\approx 0.05\text{Å}$  of systematic error. Because the majority of our spectra have modest resolution ( $R \sim 2000$ ), the metal-line transitions are typically unresolved and a simple Gaussian fit to the observed profiles would yield similar values for the equivalent widths.

The rest-frame equivalent width measurements and errors for C II 1334 and C IV 1548 ( $W_{1334}, W_{1548}$ ) are presented in Table 2. Positive detections are considered those with  $W > 3\sigma$  and non-detections are reported as  $2\sigma$  limits or the measured value if  $2\sigma < W < 3\sigma$ . Our analysis focuses on these two transitions because they span a wide range of ionization states (the ionization potentials to produce these ions are 11.3 eV and 47.9 eV respectively) and are two of the strongest lines commonly available in our sample. Note that for the strongest C IV systems ( $W_{1548} > 1\text{Å}$ ), the C IV 1548 transition is frequently blended with the C IV 1550 transition and one may adopt an additional 15% error in the  $W_{1548}$  measurement (not included explicitly in our analysis). Similarly, there may be weak and unresolved C II\* 1335 absorption present (e.g. QPQ3) that contributes to the  $W_{1334}$  measurements.

Figure 1 presents scatter plots of the  $W_{1334}$  and  $W_{1548}$  measurements against projected quasar pair separation  $R_{\perp}$ , calculated at  $z_{\text{fg}}$ . Filled symbols indicate positive,  $3\sigma$  detections. The number of detections per logarithmic  $R_{\perp}$  interval is roughly constant to 1 Mpc. The number of pairs, however, increases rapidly with increasing  $R_{\perp}$  indicating a declining detection rate. Overplotted on the figure are the unweighted mean<sup>6</sup> and RMS of the equivalent widths in bins of  $R_{\perp}$  (see also Table 3). These were calculated from the actual measurements, not the limits (e.g. negative EWs were permitted and included). Both transitions exhibit a monotonic decline in the average EW with increasing  $R_{\perp}$ , although the averages still exceed  $0.1\text{Å}$  even at  $R_{\perp} \sim 1$  Mpc. This is partly due to the few positive detections with  $W > 0.5\text{Å}$  but even after eliminating those measurements the average EWs exceed<sup>7</sup>  $0.1\text{Å}$  at all  $R_{\perp}$ . Of course, a non-zero mean is ex-

pected if not required, especially given the large analysis windows adopted from our analysis. This occurs because of the high incidence of intervening systems (especially for C IV) and the coincidence of absorption-lines from unrelated systems (an effect we minimized by excluding strongly-blended systems). That is, even ‘random’ spectral regions should exhibit a non-zero mean equivalent width. In later sections, we examine whether the quasar pair measurements exceed such random expectation.

Statistically, a generalized Kendall’s tau test, which accounts for upper limits in the EW measurements, gives a  $> 99.99\%$  probability that the null hypothesis of no correlation between  $W_{1334}$  (or  $W_{1548}$ ) and  $R_{\perp}$  is ruled out. We conclude that the observed absorption is at least statistically (if not physically) associated to the f/g quasar environment. We further explore evolution in the metal-line absorption by comparing the combined distribution of measurements and upper limits in bins of  $R_{\perp}$  (Figure 2). Regarding C II 1334, the  $W_{1334}$  distributions are nearly identical for the two bins spanning  $R_{\perp} = 0 - 200$  kpc revealing strong, low-ion absorption even beyond the estimated virial radii of the dark matter halos hosting  $z \sim 2$  quasars ( $r_{\text{vir}}^{\text{QPQ}} = 160$  kpc; see the Introduction). Beyond 200 kpc, the incidence of strong C II 1334 absorption drops sharply, even suddenly. Furthermore, the two outer bins show very similar distributions (at  $W_{1334} \approx 0.1\text{Å}$ ) with the difference driven primarily by the difference in data quality and therefore the upper limit values for the non-detections (i.e., a comparison is fair only for EW values above the detection limit). This dominates the behavior in the  $W_{1334}$  distribution at low values. We conclude that the CGM of galaxies hosting  $z \sim 2$  quasars is significantly enriched and also sufficiently self-shielded from the EUVB to show substantial C II absorption (e.g. Werk et al. 2013). We further conclude that this cool and enriched medium extends to  $R_{\perp} \approx 200$  kpc and beyond that separation there is a significant decrease in enrichment, a sharp decline in the total gas surface density, and/or an increase in the ionization level of the gas.

At the smallest  $R_{\perp}$  (less than 100 kpc), the results are similar for C IV 1548, i.e. there is a preponderance of

<sup>6</sup> We also considered the mean weighted by the square inverse of the error in the equivalent width measurements. This gives qualitatively similar results but smaller values and uncertainties that do not accurately reflect the sample variance.

<sup>7</sup> We were concerned that these averages were biased high by

errors in continuum placement, but see the analysis of stacked profiles below.

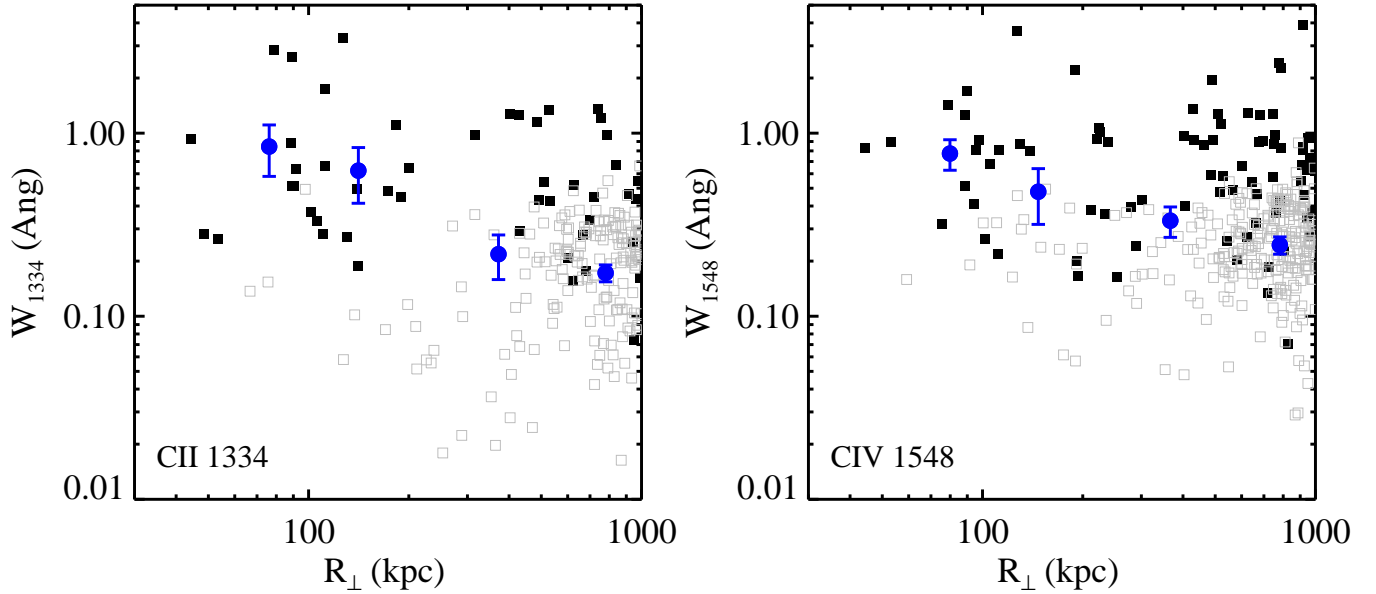


FIG. 1.— Rest-frame equivalent widths for C II 1334 (left) and C IV 1548 (right) measured at  $z \approx z_{\text{fg}}$  of the f/g quasar in our quasar pair sample, restricted to the analysis of spectra outside the Ly $\alpha$  forest of the b/g quasar. These are plotted against the projected pair separations  $R_{\perp}$ , measured at  $z_{\text{fg}}$ . Detections ( $3\sigma$ ) are the filled black symbols and non-detections are open gray squares, plotted at their  $2\sigma$  values. The blue symbols express the average  $W_{\lambda}$  values and RMS scatter, taking non-detections at their measured values (i.e. column 7 in Table 2) in bins of  $R_{\perp} = [0, 100], [100, 200], [200, 500], [500, 1000]$  kpc. Both transitions exhibit large equivalent widths ( $W_{\lambda} \approx 1\text{\AA}$ ) at the smallest impact parameters. Both distributions also exhibit an anti-correlation with  $R_{\perp}$  (at  $> 99.99\%$  confidence). We conclude that  $z \sim 2$  quasars are enveloped in a highly enriched, circumgalactic medium.

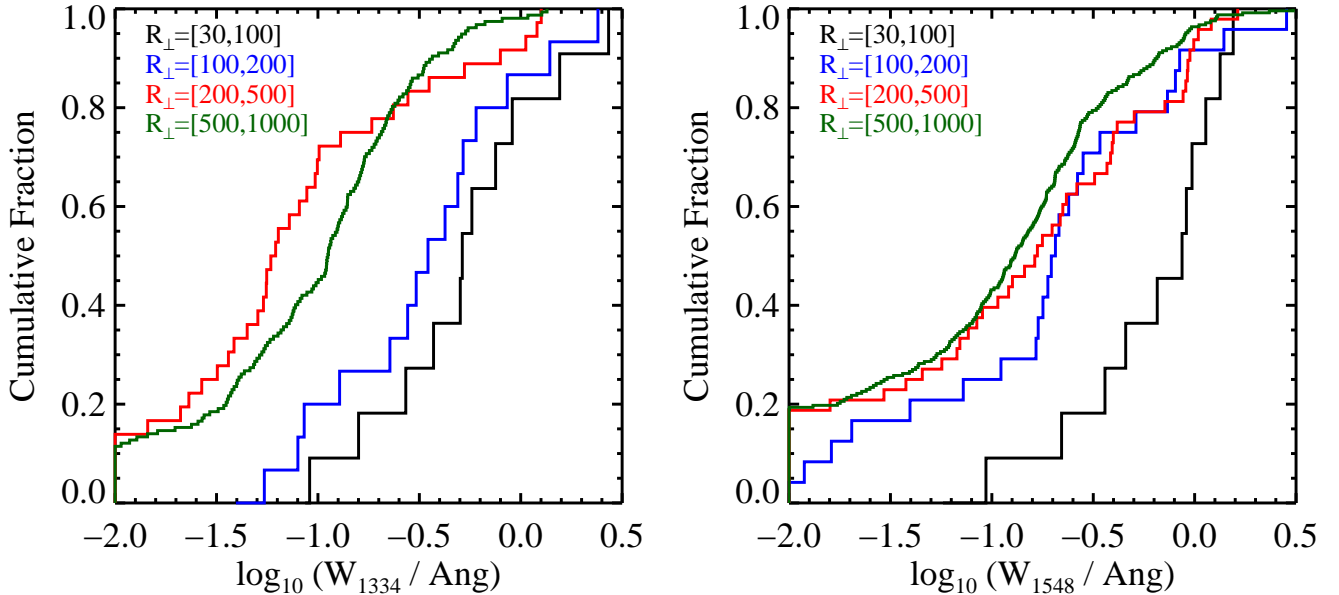


FIG. 2.— Cumulative distributions of the rest-frame equivalent width measurements for C II 1334 (left) and C IV 1548 (right) in bins of  $R_{\perp}$ . For C II 1334, we find much higher  $W_{1334}$  values for  $R_{\perp} < 200$  kpc with little dependence below this impact parameter. This implies a cool and enriched CGM on scales characteristic of the estimated virial radius  $r_{\text{vir}}^{\text{QFQ}} \approx 160$  kpc. In contrast, the C IV 1548 equivalent widths are lower at  $R_{\perp} > 100$  kpc but then decline less rapidly to larger  $R_{\perp}$ . This implies that beyond  $r_{\text{vir}}$ , the gas remains enriched on average but becomes more highly ionized. Note that the distributions begin at non-zero values owing to the sensitivity limit of the spectra.

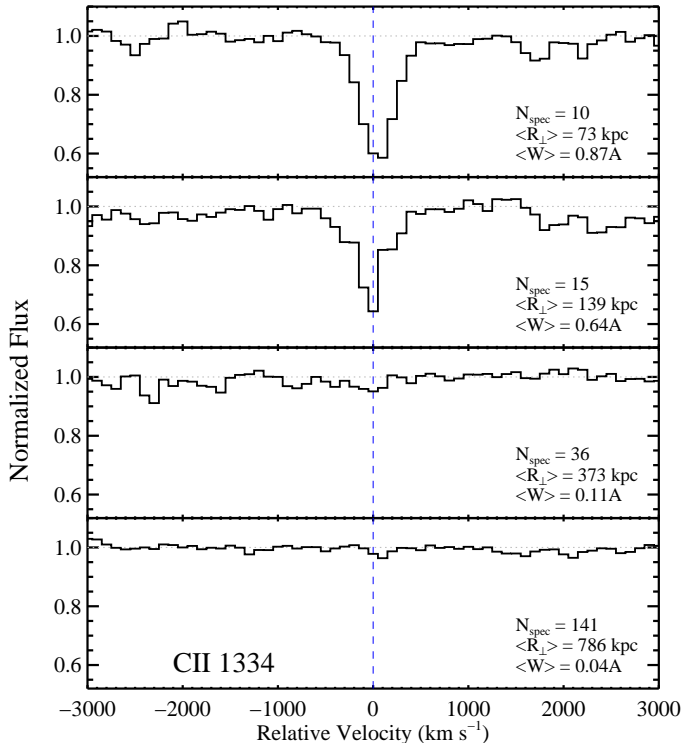


FIG. 3.— Average absorption-line spectra for C II 1334 in bins of  $R_{\perp} = [0, 100], [100, 200], [200, 500], [500, 1000]$  kpc, stacked at  $v = 0 \text{ km s}^{-1}$  corresponding to the strongest Ly $\alpha$  absorber within  $1500 \text{ km s}^{-1}$  of  $z_{\text{fg}}$  ( $z_{\text{Ly}\alpha}$ ; defined in QPQ6). One observes large, average equivalent widths at  $R_{\perp} < 200$  kpc and the disappearance of C II absorption at larger separations. Note that the strong absorption ( $W_{1334} \gtrsim 0.5 \text{ \AA}$ ) is not driven by a small set of events; a median stack yields qualitatively similar results. The equivalent widths reported were measured in  $\delta v = \pm 800 \text{ km s}^{-1}$  windows. The uncertainty is dominated by sample variance in the first two bins (we estimate a 20% error) and by a combination of statistical and systematic error (continuum fitting) for the larger  $R_{\perp}$  intervals. We estimate  $50 \text{ m\AA}$  and  $30 \text{ m\AA}$  for the highest  $R_{\perp}$  intervals.

strong absorption ( $W_{1548} \gtrsim 1 \text{ \AA}$ ). The incidence modestly decreases for  $R_{\perp} = [100, 200]$  kpc and also as one extends to  $R_{\perp} = [200, 500]$  kpc (again, the differences at  $W_{1548} < 0.1 \text{ \AA}$  are driven by differences in the spectral S/N). We stress, however, that there is no statistically significant difference in the distribution for these two intervals. Comparing to the C II 1334 measurements, the results indicate that the gas in the quasar environments extending to  $R_{\perp} \approx 500$  kpc remains substantially enriched in carbon but that the average ionization state is significantly higher in the outer regions. Of course, this material is unlikely to be physically bound to the quasar host, or to have originated from within it, but may be associated to neighboring galaxies in the extended environment. We explore this result further in the following sections.

The trends described above may be further illustrated by constructing average (i.e. stacked) profiles in bins of  $R_{\perp}$ . Figures 3 and 4 show the stacked spectra for C II 1334 and C IV 1548 with  $v = 0 \text{ km s}^{-1}$  corresponding to  $z = z_{\text{Ly}\alpha}$ , the approximate redshift centroid of the strongest H I Ly $\alpha$  absorption within a  $3000 \text{ km s}^{-1}$  window centered on  $z_{\text{fg}}$  (QPQ6). To generate the stacks, we rebinned each original spectrum onto a grid centered on  $v = 0 \text{ km s}^{-1}$  with a dispersion of  $\delta v = 100 \text{ km s}^{-1}$ . The

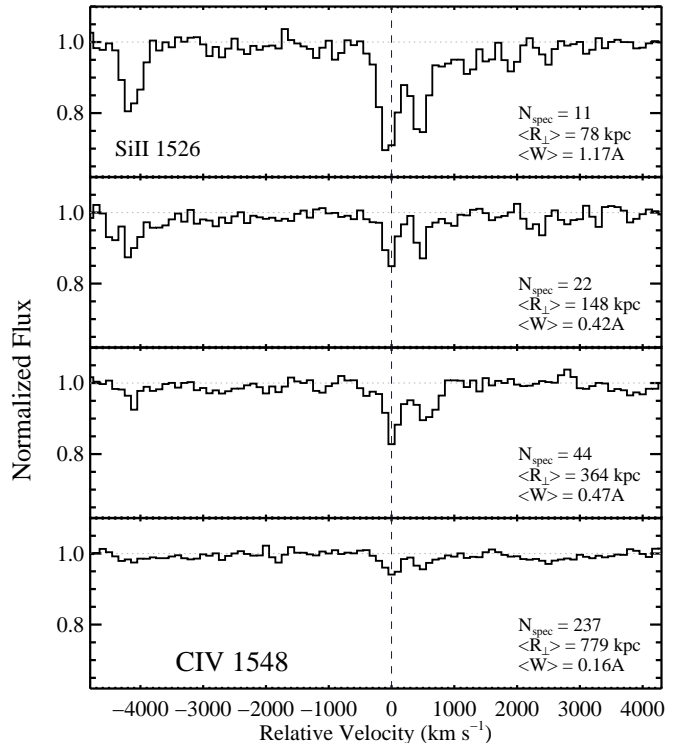


FIG. 4.— Same as for Figure 3 but for C IV 1548. In this case one also observes absorption from C IV 1550 at  $v \approx +500 \text{ km s}^{-1}$  and Si II 1526 at  $v \approx -4200 \text{ km s}^{-1}$ . In contrast to C II 1334, the average C IV 1548 absorption remains substantial to  $R_{\perp} \approx 500$  kpc.

average was taken with uniform weighting of the pairs. For this analysis, we did not include transitions flagged as having blends with other, coincident absorption lines. Lastly, a low-amplitude (i.e. near unit value), low-order polynomial was used to normalize the resultant stacks which we associate to small errors in the continuum normalization.

The averaged profiles exhibit strong C II 1334 absorption for  $R_{\perp} < 200$  kpc which essentially vanishes at larger impact parameters (there is a weak ‘line’ with  $W_{1334} \approx 0.2 \text{ \AA}$  present at  $R_{\perp} > 200$  kpc). These trends, of course, follow the results observed for the individual  $W_{1334}$  measurements. Turning to C IV 1548, we observe strong absorption from both members of the C IV doublet to  $R_{\perp} = 500$  kpc, and then weaker but non-negligible absorption for  $R_{\perp} = [500, 1000]$  kpc. Again, the striking difference with the C II 1334 results is the sustained, strong absorption to well beyond 200 kpc. Statistically, the extended environments of quasars is substantially enriched to distances greatly exceeding the virial radius of the host dark matter halo. We further emphasize that this cannot be simple ISM gas from neighboring galaxies, the H I column densities are far too low. Such galaxies may, however, be the source of this enrichment. In the largest  $R_{\perp}$  interval gas unassociated with the f/g quasar but within our  $\Delta v = \pm 1500 \text{ km s}^{-1}$  window contributes to the signal. As discussed in the Appendix, the random incidence of C IV systems with  $W_{1548} > 0.3 \text{ \AA}$  is 2.1 absorbers per  $\Delta z = 1$  interval at  $z_{\text{abs}} \approx 2.1$ . Within our  $3000 \text{ km s}^{-1}$  window, we expect 0.065 systems on average giving  $W_{1548} \approx 0.05 \text{ \AA}$ . This represent approximately one-third of the signal in our largest bin. The C IV stacks also exhibit significant

TABLE 3  
QPQ7 AVERAGE EQUIVALENT WIDTH VALUES

$R_{\perp}^{\min}$ (kpc)	$R_{\perp}^{\max}$ (kpc)	$m_{\text{pair}}^a$	$\langle R_{\perp} \rangle$ (kpc)	$W_{1334}$ (Å)	$\sigma(W)^b$ (Å)	$m_{\text{pair}}^a$	$\langle R_{\perp} \rangle$ (kpc)	$W_{1548}$ (Å)	$\sigma(W)^b$ (Å)
30	100	12	76	0.84	0.26	12	80	0.79	0.15
100	200	16	141	0.63	0.21	25	147	0.48	0.16
200	500	37	372	0.21	0.06	49	367	0.33	0.06
500	1000	158	780	0.17	0.02	249	781	0.24	0.03

NOTE. — Equivalent width values are rest-frame measurements.

<sup>a</sup> Number of pairs analyzed.

<sup>b</sup> Calculated from the dispersion of the individual measurements. We also estimate an additional systematic uncertainty of 20% from continuum placement.

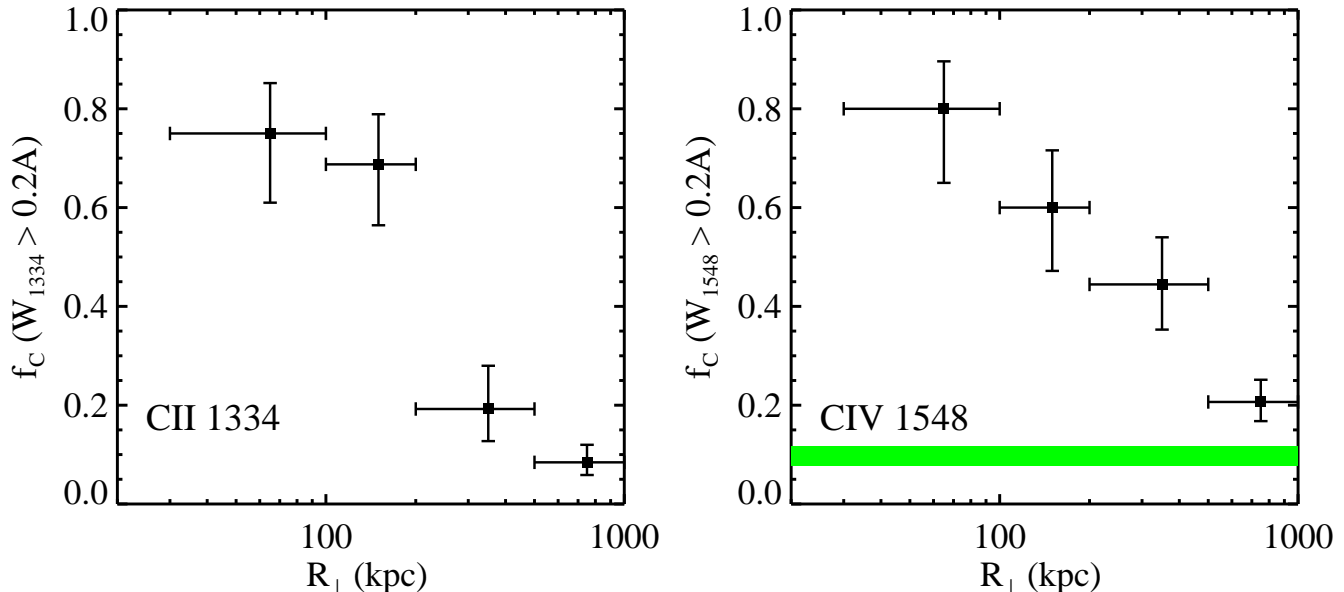


FIG. 5.— Covering fractions  $f_C$ , estimated from the fraction of pairs exhibiting  $W_{\lambda} > 0.2\text{\AA}$ , in bins of impact parameter  $R_{\perp}$  for (a) C II 1334 and (b) C IV 1548. These provide another perspective on the chief results of this work: (i) strong and nearly ubiquitous C II 1334 absorption to  $R_{\perp} \approx 200$  kpc followed by a rapid drop-off; (ii) a more gradual decline in the incidence and strength of C IV 1548 absorption. In panel (b), the green band shows an estimate of the covering fraction for random  $3000 \text{ km s}^{-1}$  intervals in the IGM based on our  $\ell(z)$  measurement (see the Appendix).

absorption at  $v \approx -4200 \text{ km s}^{-1}$ , corresponding to the low-ion Si II 1526 transition. Its behavior qualitatively tracks the trends observed for C II 1334, as expected.

#### 4. RESULTS

##### 4.1. Covering Fractions ( $f_C$ )

To further characterize the metal-absorption associated with the measurements of galaxies hosting  $z \sim 2$  quasars and to facilitate comparisons to CGM research for other galaxy samples and epochs, we have made estimates for the covering fractions  $f_C$  of the gas as a function of  $R_{\perp}$ . These are calculated simply by taking the ratio of the pairs where the EW measurements exceed a given threshold to the total number. Uncertainties are estimated from a standard Wilson score. Before presenting the results, we emphasize that the  $f_C$  values recovered are sensitive to both the assumed  $R_{\perp}$  bins and the (rather arbitrary) equivalent width limit  $W^{\text{lim}}$ . For the former, we maintain the  $R_{\perp}$  intervals presented in the previous section which are a compromise between bin-width and sample size. For  $W^{\text{lim}}$ , we are driven primar-

ily by data quality. In the following we present results for  $W^{\text{lim}} = 0.2\text{\AA}$  and restrict the analysis to the spectra satisfying  $\sigma(W) \leq 0.1\text{\AA}$  (134 pairs for C II 1334 and 135 pairs for C IV 1548), i.e. we adopt a  $2\sigma$  detection threshold.

Figure 5a present the  $f_C$  measurements for C II 1334 (see also Table 4). The covering fraction is near unity for  $R_{\perp} < 200$  kpc, consistent with previous results that the CGM of quasar hosts exhibits a high covering fraction to gas that is optically thick at the H I Lyman limit (QPQ1, QPQ2, QPQ5, QPQ6). Indeed, these strong C II 1334 detections contributed in part to those prior conclusions because we adopted strong C II 1334 as an indicator that the gas is optically thick. Independently, we conclude that the gas is significantly enriched in heavy elements. Furthermore, the steep drop in  $f_C^{1334}$  at  $R_{\perp} > 200$  kpc requires that this  $\text{C}^+$  gas lies predominantly within the host halo. The extent, however, well exceeds any reasonable estimations for the ISM of the host galaxy and very few sightlines exhibit H I columns reflective of ISM gas

TABLE 4  
QPQ7  $f_C$  VALUES

$R_{\perp}^{\min}$ (kpc)	$R_{\perp}^{\max}$ (kpc)	$m_{\text{pair}}^a$	$f_C^{1334}$	$+1\sigma^b$	$-1\sigma^b$	$m_{\text{pair}}^a$	$f_C^{1548}$	$+1\sigma^b$	$-1\sigma^b$
$W_{\text{lim}} = 0.2\text{\AA}$									
30	100	12	0.75	0.14	0.10	10	0.80	0.15	0.10
100	200	16	0.69	0.12	0.10	15	0.60	0.13	0.12
200	500	27	0.19	0.06	0.08	27	0.44	0.09	0.10
500	1000	83	0.08	0.03	0.04	92	0.21	0.04	0.04
$W_{\text{lim}} = 0.3\text{\AA}$									
30	100	12	0.58	0.14	0.13	12	0.83	0.13	0.08
100	200	16	0.56	0.12	0.12	19	0.32	0.09	0.11
200	500	33	0.15	0.05	0.07	38	0.34	0.07	0.08
500	1000	138	0.08	0.02	0.03	170	0.15	0.03	0.03

<sup>a</sup> Number of pairs analyzed.

<sup>b</sup> Confidence limits from Binomial statistics (Wilson score) for a 68% interval.

(QPQ6). Instead, this material must be halo gas<sup>8</sup>. We also emphasize that  $0.2\text{\AA}$  well exceeds the average equivalent width for C II 1334 in ‘random’ LLS ( $\approx 0.06\text{\AA}$ ), at  $z \approx 3$  with  $N_{\text{HI}} = 10^{17} - 10^{19} \text{ cm}^{-2}$  Fumagalli et al. (2013). The gas probed here represents a more highly enriched and/or dynamic medium than ‘typical’, optically thick gas.

Regarding  $f_C$  for C IV 1548, the results follow the conclusions drawn in the previous section, i.e. that the C IV 1548 absorption extends to  $\approx 500 \text{ kpc}$  with a declining incidence that is shallower than that observed for C II 1334. The results are well-described by a single power-law,  $f_C^{1548}(W > 0.2\text{\AA}) \sim 0.4(R_{\perp}/300 \text{ kpc})^{1/2}$ . In the following sub-section, we measure the cross-correlation function between C IV and quasars, finding enhanced absorption to at least 1 Mpc.

#### 4.2. C IV-Quasar Two-Point Cross-correlation

The results presented above demonstrate clearly that the environments surrounding the host galaxies of luminous  $z \sim 2$  quasars exhibit an excess of C IV absorption to scales of at least 500 kpc. We may quantify the excess by estimating the two-point cross-correlation function between C IV absorbers and quasars,  $\xi_{\text{CIV-Q}}$ . Our approach follows the maximum likelihood methodology presented in QPQ2 and QPQ6 used to assess the cross-correlation of H I absorption to quasars. To briefly summarize, we parameterize  $\xi_{\text{CIV-Q}}(r)$  as a power-law  $(r/r_0)^{-\gamma}$ , project the 3D correlation function along the quasar sightlines to determine the transverse correlation function  $\chi_{\perp}(R_{\perp})$ , and find the values of  $r_0$  and  $\gamma$  which maximize the likelihood of recovering the observed incidence of strong C IV absorbers with  $R_{\perp}$ . Following standard convention for clustering analysis, the calculations are performed and reported in comoving coordinates in units of  $h^{-1} \text{ Mpc}$  with  $H_0 = 100 h^{-1} \text{ km s}^{-1} \text{ Mpc}^{-1}$ .

Central to the evaluation of  $\xi_{\text{CIV-Q}}$  is a precise and accurate estimate for the incidence of ‘random’ C IV absorbers along quasar sightlines. And, in our analysis this background may contribute significantly because of the large uncertainty in quasar redshifts which requires that

we evaluate  $\chi_{\perp}$  over relatively large velocity windows around each f/g quasar ( $\Delta v = \pm 1500 \text{ km s}^{-1}$ ). While a number of C IV surveys have been previously performed (Boksenberg et al. 2003; D’Odorico et al. 2010; Cooksey et al. 2013), none of these is entirely satisfactory for the C IV equivalent widths characterizing our study (i.e.  $W_{1548} \approx 0.5\text{\AA}$ ). Therefore, we carried out our own survey for strong C IV systems, as described in the Appendix. The primary result is a ‘random’ incidence for strong C IV absorbers (per unit redshift;  $W_{1548} > 0.3\text{\AA}$ ) of  $\ell(z)_{\text{CIV}} = 2.1$  at  $\langle z \rangle \approx 2.1$  with a 10% statistical uncertainty and a comparable, estimated systematic error. We assume no redshift evolution in  $\ell(z)_{\text{CIV}}$ ; Cooksey et al. (2013) find a small ( $\approx 30\%$ ) decrease in  $\ell(z)_{\text{CIV}}$  from  $z = 2$  to 3.

A key consideration for the analysis is the limiting equivalent width  $W_{\text{CIV}}^{\text{lim}}$  for systems in the correlation analysis. In the previous section, we presented covering fraction results for  $W_{\text{CIV}}^{\text{lim}} = 0.2\text{\AA}$ . For the following, we take  $W_{\text{CIV}}^{\text{lim}} = 0.3\text{\AA}$  and require a  $3\sigma$  detection at this equivalent width limit. This is a stricter definition and is also motivated by our requirement to have a well-measured incidence of ‘random’ C IV absorbers. In addition, we restrict to pairs where  $z_{\text{fg}} < 3.5$ . The sample encompasses 137 pairs with  $\langle z_{\text{fg}} \rangle = 2.34$  and comoving impact parameter  $R_{\perp}^{\text{com}}$  ranging from 0.9 to 2.6  $h^{-1} \text{ Mpc}$ .

The results of our maximum likelihood analysis<sup>9</sup> for  $r_0$  and  $\gamma$  are presented in Figure 6. We recover  $r_0 = 7.5_{-1.4}^{+2.8} h^{-1} \text{ Mpc}$  and  $\gamma = 1.7_{-0.2}^{+0.1}$  with degeneracy between the two parameters. The contours exhibit a sharp cutoff on the right-hand side (larger  $r_0$ ) where the models predict the detection of at least one C IV absorber at an impact parameter where none was found. Our best-fit  $\gamma$  values follow results reported previously for galaxy-galaxy clustering, as predicted from analysis of dark matter halo clustering in numerical simulations (e.g. Mo & White 1996). This suggests that the C IV gas may be associated to dark matter halos in the quasar vicinity, i.e. the CGM of neighboring galaxies clustered to the quasar host. The large correlation length, meanwhile, reflects both the mass of the quasar host galaxy but also

<sup>8</sup> Including material associated to satellite galaxies.

<sup>9</sup> See QPQ2 and QPQ6 for details on the methodology.

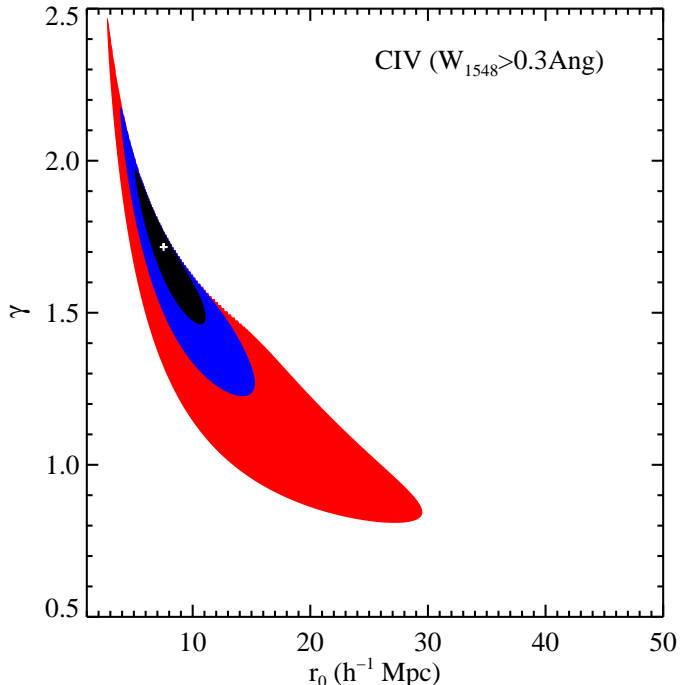


FIG. 6.— Constraints on the cross-correlation function for strong ( $W_{1548} > 0.3\text{\AA}$ ) C IV 1548 absorption and quasars at  $z \approx 2.5$ , parameterized as  $\xi_{\text{CIV-Q}}(r) = (r/r_0)^{-\gamma}$ . The best-fit values are  $\gamma = 1.7^{+0.1}_{-0.2}$  and  $r_0 = 7.5^{+2.8}_{-1.4} h^{-1} \text{ Mpc}$ , with degeneracy between the two. For  $\gamma = 1.6$ , typical of galaxy-galaxy and galaxy-quasar clustering, the data demand  $r_0 > 5h^{-1} \text{ Mpc}$  at 95% confidence. The colors (black, blue, red) describe contours of (1,2,3) $\sigma$  confidence levels.

implies the C IV gas occurs preferentially near massive halos (similar to our inferences on LLS in QPQ6). We explore this assertion further in the next section.

Figure 7 presents a binned evaluation of the transverse, projected cross-correlation function  $\chi_{\perp}(R, \Delta v)$  for the quasar pair sample and the best-fit model with a band illustrating the uncertainty in  $r_0$ . Clearly, this model provides a good description of the data. We conclude that strong C IV systems are highly clustered to quasars at  $z \sim 2$  with a clustering amplitude  $r_0 \approx 7.5h^{-1} \text{ Mpc}$ .

## 5. DISCUSSION

In this section, we consider the implications of our results for the ICM, the origin of the CGM, and the nature of strong metal-line absorbers. Before proceeding, we present the results from a simple series of photoionization calculations made with the Cloudy software package (v10; Ferland et al. 2013), to offer physical insight into our observations. Figure 8 shows the predicted ionic fractions  $f_i \equiv N_i/N$  and ionic column densities  $N_i$  of  $\text{C}^+$  and  $\text{C}^{3+}$  for a plane-parallel gas slab with total hydrogen column densities  $N_{\text{H}} = 10^{19.5}, 10^{20}$  and  $10^{21} \text{ cm}^{-2}$ , metallicity  $[\text{C}/\text{H}] = -1$ , and an assumed EUVB background from the CUBA package ( $z = 2$ ; Haardt & Madau 2012) with a range of ionization parameters  $U \equiv \Phi/cn_{\text{H}}$ . At low  $U$  values ( $\log U < -2.5$ ), the lower ionization state dominates and one predicts a modest  $\text{C}^{3+}$  column density, consistent with our observations. From a C II 1334 equivalent width of  $W_{1334} = 1\text{\AA}$ , one conservatively estimates a column density  $N(\text{C}^+) > 10^{14.7} \text{ cm}^{-2}$  from the linear curve-of-growth approximation. For  $[\text{C}/\text{H}] = -1$ , this

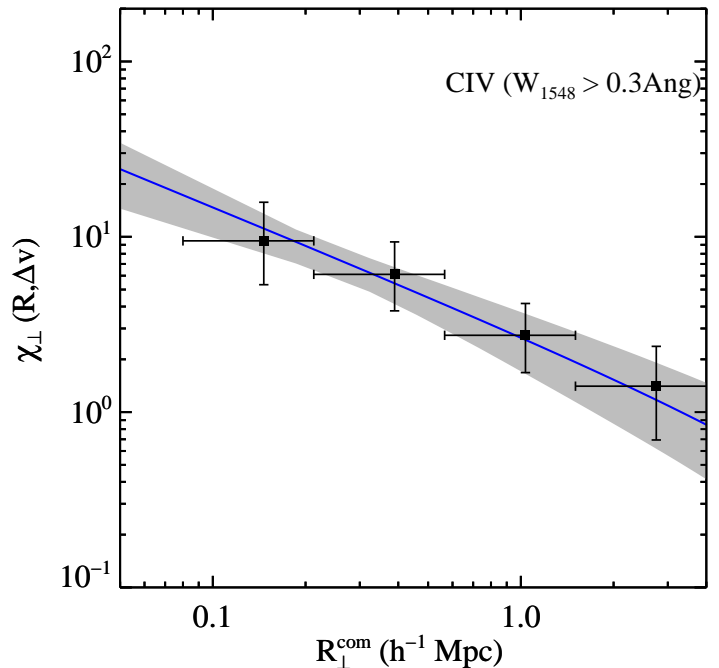


FIG. 7.— Projected cross-correlation function between strong C IV absorbers and quasars, estimated in arbitrary bins of  $R_{\perp}^{\text{com}}$ . Overplotted on these values is the best-fit model from a maximum likelihood analysis  $\xi_{\text{CIV-Q}}(r) = (r/r_0)^{-\gamma}$  (blue line;  $r_0 = 7.5^{+2.8}_{-1.4} h^{-1} \text{ Mpc}$ ,  $\gamma = 1.7^{+0.1}_{-0.2}$ ), and our estimate of the  $1\sigma$  uncertainties. This model provides a good description of the observations.

implies  $N_{\text{H}} > 10^{20} \text{ cm}^{-2}$ . Such models also reproduce the large  $N_{\text{HI}}$  values observed in the QPQ sample (QPQ6). The figure also demonstrates that one can reproduce systems with strong C IV 1548 absorption and negligible C II 1334, characteristic of gas at large impact parameters from the quasar hosts, provided  $N_{\text{H}} \approx 10^{20} \text{ cm}^{-2}$  and  $\log U \gtrsim -2$ . This implies a medium whose volume density decreases with radius but with a roughly constant surface density.

### 5.1. Constraining Enrichment Models for the ICM

One motivation for our analysis was to test the prediction that massive galaxies expel a large mass in metals at early times to reproduce  $z < 1$  observations of the ICM (Renzini et al. 1993; Matteucci & Gibson 1995; Arrigoni et al. 2010; Yates 2014). Taking one recent calculation as a fiducial example, the preferred model of Yates (2014) predicts that a  $10^{12.5} M_{\odot}$  galaxy at  $z = 2$  will have ejected several  $10^9 M_{\odot}$  in metals by  $z = 2$ . In this model, the early enrichment and feedback is dominated by massive stars. We may then compare these predictions to estimates for the metal mass surrounding the massive,  $z \sim 2$  galaxies of the QPQ survey.

The results presented in Figures 1 and 5 imply a large mass of metals traced by C II 1334 in the halos of  $z \sim 2$ , massive galaxies. To provide a preliminary and rough estimate for this mass, consider the following calculation which gives a conservative, lower limit to the metal mass: (i) convert the individual  $W_{1334}$  values into  $\text{C}^+$  column densities  $N(\text{C}^+)$  conservatively assuming the linear curve-of-growth (COG) approximation (e.g. Spitzer 1978). This includes negative values (i.e. all

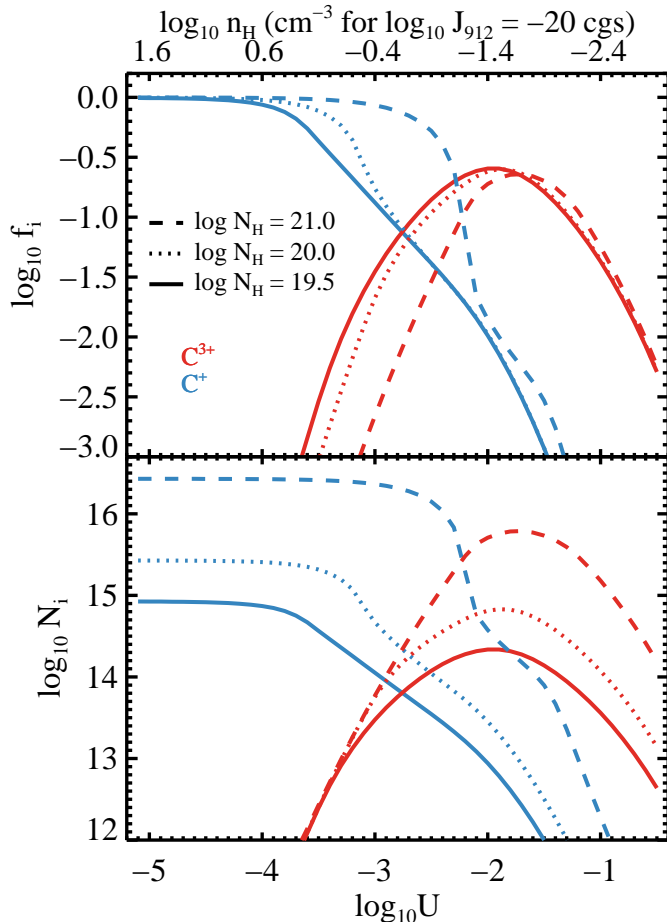


FIG. 8.— (top): Ionization fractions  $f_i = N_i/N$  for  $C^+$  (blue) and  $C^{3+}$  (red) as a function of ionization parameter  $U$  and total hydrogen column density  $N_H$ . All models assume a standard EUVB radiation field at  $z = 2$  and a gas metallicity  $[C/H] = -1$ . At  $\log U = -3$ , which we believe is representative of the cool CGM (QPQ3, QPQ8),  $C^+$  has  $f_i = 0.1 - 0.3$  and  $C^{3+}$  shows  $f_i < 0.1$ . This is consistent with the stronger C II 1334 absorption observed relative to C IV 1548 (Figure 1; QPQ5). The top axis is labeled by the number density  $n_H$  assuming an intensity for the EUVB at the Lyman limit  $J_{912} = 10^{-20} \text{ erg s}^{-1} \text{ cm}^{-2} \text{ Hz}^{-1}$ . (bottom): The predicted column densities  $N_i$  as a function of  $\log U$  and  $N_H$ . These photoionization models predict  $N(C^+) > N(C^{3+})$  for  $\log U < -2.5$ . From the  $C^+$  column densities estimated, one requires  $N_H > 10^{20} \text{ cm}^{-2}$ . The figure also demonstrates that in gas where only C IV 1548 is detected, one expects  $\log U \gtrsim -2$ .

non-detections); (ii) average these  $N(C^+)$  values in bins of  $R_\perp$  with 5 measurements in each bin,  $\langle N(C^+) \rangle$ ; (iii) calculate the mass in the  $i$ th annulus defined by the  $i$ th set of 5 pairs,  $M_i = \langle N(C^+) \rangle_i m_C \pi [R_{i,max}^2 - R_{i,min}^2]$  and; (iv) assume that carbon represents 20% of the total estimated metal mass, as in our Sun.

The cumulative mass profile, plotted relative to the virial radius, is shown as the solid black curve in Figure 9. This represents a very conservative lower limit to the metal mass of the cool CGM phase because we have ignored line-saturation and because  $C^+$  is likely only a small fraction of all C ( $< 50\%$ ; Figure 8), even in this cool phase. Nevertheless, the total mass  $M_{\text{metal}}^{\text{cool}}$  is substantial: approximately  $5 \times 10^6 M_\odot$  at the estimated virial radius and nearly  $10^7 M_\odot$  at  $R_\perp = 200 \text{ kpc}$ . This is comparable to the metal mass in a  $10^{10} M_\odot$  gas with

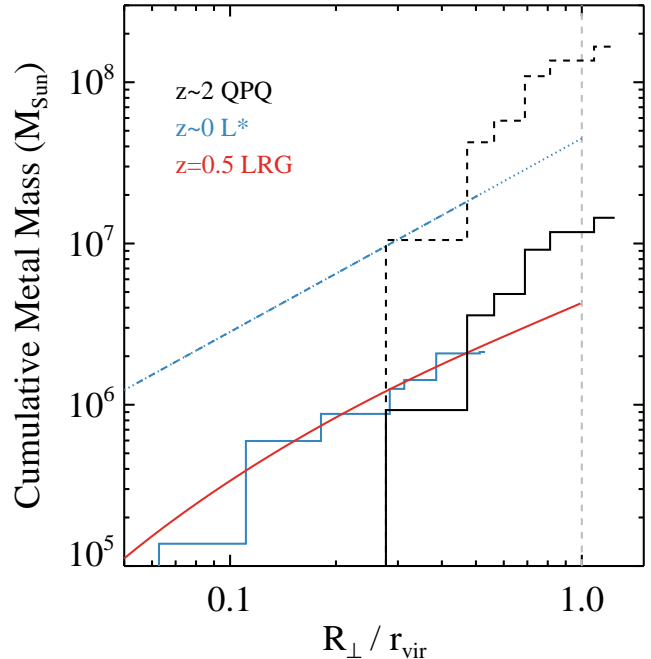


FIG. 9.— Estimated cumulative mass profiles for the cool CGM of several galaxy populations:  $z \sim 2$  massive galaxies (black; QPQ), luminous  $z \sim 0$  galaxies (red; Werk et al. 2014), and LRGs (blue; Z14). The solid curves offer very conservative (i.e. lower limit) estimates based on saturated absorption and no ionization corrections (see § 5.1 for details). The dashed curves present estimates that include ionization corrections (Werk et al. 2014) and the dotted curve represents the extrapolation of such analysis. Comparing results that adopt the same set of assumptions (i.e. restricting comparison to curves with the same line-style), we find that the total mass at  $r_{\text{vir}}$  is highest in the halos of  $z \sim 2$  massive galaxies.

$1/10$  solar metallicity<sup>10</sup>, and we stress again that this estimate gives a very conservative lower limit to  $M_{\text{metal}}^{\text{cool}}$ . While in principle the ISM of satellite galaxies will contribute to this estimate, none of these sightlines exhibit H I column densities characteristic of a galactic ISM (i.e.  $N_{\text{HI}} > 10^{20} \text{ cm}^{-2}$ ). And, the high covering fraction of C II 1334 absorption implies a widespread CGM (Figure 11) that cannot be easily explained by satellites (e.g. QPQ3 Tumlinson et al. 2013).

To provide a better estimate for the metal mass, we further assume the following: (v) the QPQ sightlines with  $W_{1334} > 0.2 \text{ \AA}$  require a (conservative) 0.3 dex correction to their COG-estimated  $N(C^+)$  values. This is based on analysis of ions that exhibit multiple transitions with a wide range of oscillator strengths (e.g. Fe II); (vi)  $C^+$  represents only 1/3 of the total C in this cool phase (i.e.  $\log U \approx -3$ ; Figure 8); and (vii) C/O is subsolar by a factor of 2, as observed in metal-poor stars (Akerman et al. 2004), such that C represents only 10% of the total mass in metals. The second correction ( $C^+/C = 1/3$ ) is supported by detailed photoionization modeling of the gas from observed ionic ratios (QPQ3, QPQ8). Meanwhile, the saturation correction is still conservative given the very large  $W_{1334}$  measurements. Together, these corrections imply  $\approx 10\times$  more metal mass in the cool CGM, i.e.  $M_{\text{CGM}}^{\text{cool}}$  exceeds  $10^8 M_\odot$  at  $\approx r_{\text{vir}}$ , and we

<sup>10</sup> One may also infer this mass by the fact that strong C II absorption implies  $N_{\text{HI}} > 10^{18} \text{ cm}^{-2}$ , e.g. QPQ5.

still consider this a conservative estimate.

Comparing to the predictions from chemical evolution models (e.g. Yates 2014), the cool CGM represents  $\gtrsim 10\%$  of the metals predicted to in galactic halos with  $M \approx 10^{12.5} M_{\odot}$  at  $z \approx 2$ . We conclude that the cool CGM represents a small but non-negligible fraction of the metals of the incipient intragroup/intracluster medium (IGrM/ICM). We further emphasize that a massive reservoir of hot, enriched gas could exist within the QPQ halos. The observed cool gas almost certainly requires an ambient warm/hot medium to provide pressure support (e.g. QPQ3) and such hot halos are predicted to be already ubiquitous at  $z \sim 2$  in massive halos (e.g. Fumagalli et al. 2014). Unfortunately, the far-UV diagnostics provided by the absorption spectra are insensitive to material with  $T > 10^6$  K. Even the apparent absence of strong N V and O VI absorption (QPQ3, QPQ8) would only rule out metal-enriched gas with  $T \approx 10^{5-6}$  K. Perhaps, one may offer model-dependent estimations of the hot gas by considering predictions for such ions when cool gas interacts with a hot medium (e.g. Kwak et al. 2011).

Returning to the cool CGM and its relation to the IGrM/ICM, we are motivated to examine the relative abundances within this medium (e.g., O/Fe, Si/Fe) to test competing scenarios of early enrichment and feedback (e.g. Arrighi et al. 2010; Yates 2014). This will require, however, observations with high spectral resolution and a careful treatment of ionization corrections. We defer such analysis to future work.

### 5.2. Comparing the Cool CGM to other Galaxy Populations

By drawing comparisons between the QPQ observations and other CGM measurements in galaxies with a wide range of halo mass and age, we may gain insight into the physical processes that dominate the CGM. This sub-section performs the empirical comparison and we discuss implications for physical processes in § 5.5.

A principal result of our analysis is the predominance of strong, low-ion metal absorption to  $R_{\perp} \approx 200$  kpc in the halos of galaxies hosting quasars. Strong low-ion absorption from the CGM of galaxies (aka halo gas) has been recognized previously at  $z < 1$  (e.g. Bergeron 1986; Steidel 1993; Lanzetta 1993). Indeed, there is an extensive, and still growing, literature on the incidence and nature of Mg II absorption in the CGM of luminous galaxies at  $z < 1$  (e.g. Chen et al. 2010a; Nielsen et al. 2013; Werk et al. 2013), and also the hosts of quasars at  $z \lesssim 1$  (Bowen et al. 2006; Farina et al. 2013). A primary conclusion of this literature is that strong Mg II absorption occurs at impact parameters  $R_{\perp} \lesssim 75$  kpc for  $L^*$  galaxies. There is also the indication that Mg II absorption strength correlates with galaxy luminosity and/or halo mass (Chen et al. 2010b; Churchill et al. 2013; Farina et al. 2014). We turn to our results in the context of this previous work, restricting the comparison to scales of the dark matter halo and presented in physical units (kpc).

Figure 10a presents the C II 1334 equivalent width distribution for the QPQ7 sample (black squares) compared against the set of such measurements for  $L \approx L^*$  galaxies at  $z \sim 0.2$  taken from the COS-Halos survey (red circles; Werk et al. 2013; Tumlinson et al. 2013). The loci of the

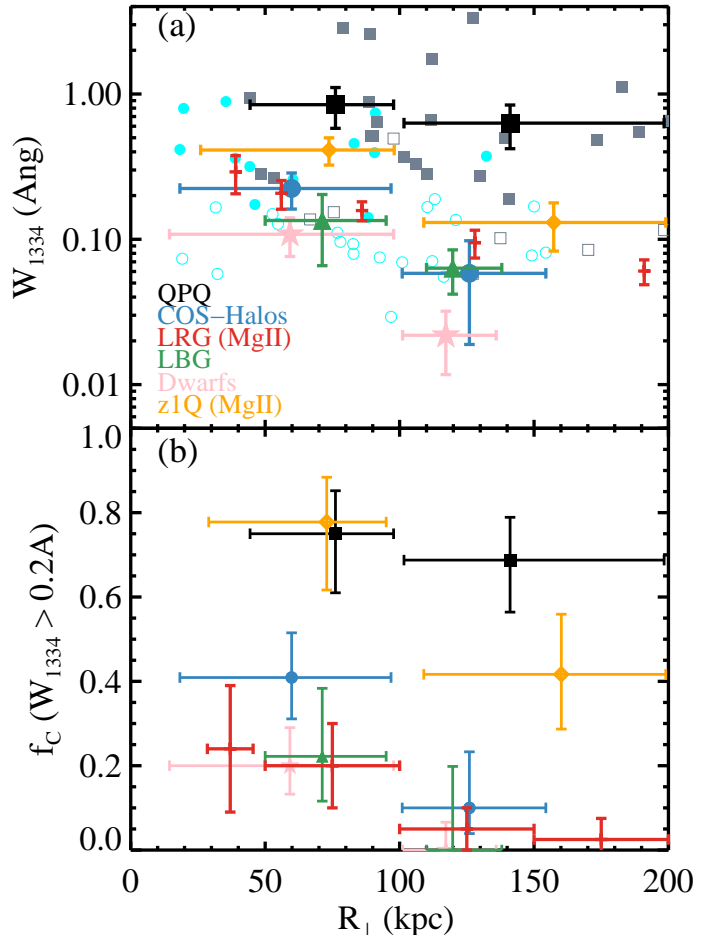


FIG. 10.— (a) Scatter plot of the rest-frame equivalent widths of C II 1334 along quasar sightlines with impact parameters  $R_{\perp}$  to the  $z \sim 2$  massive galaxies hosting quasars (black squares; this paper) and present-day  $L^*$  galaxies (blue circles; Werk et al. 2013). Although the loci of these samples overlap, the QPQ data exhibit larger values on average and a higher incidence of positive detections. The figure also shows a set of binned evaluations  $\langle W_{1334} \rangle$  for  $z \sim 0$  dwarf galaxies (pink stars; Bordoloi et al., in prep.),  $z \sim 0.5$  LRGs (red symbols; scaled from  $W_{2796}$ , see § 5.2; Z14), and the  $z \sim 2$  LBGs (green triangles; Adelberger et al. 2005a; Simcoe et al. 2006; Rudie et al. 2013; Crighton et al. 2013). It is evident that the CGM of the QPQ sample exhibits the strongest low-ion absorption of any galaxy population. This conclusion is further emphasized in panel (b) which gives the covering fraction in each sample for  $W_{1334} > 0.2 \text{ \AA}$ .

measurements overlap, but the detection rate and typical  $W_{1334}$  values are much higher for the QPQ7 sample. These differences are emphasized in the binned evaluations ( $W_{1334}$ ), and the estimated covering fractions  $f_C$  for  $W_{1334} > 0.2 \text{ \AA}$  (Figure 10b). The contrast is most striking at  $R_{\perp} = 100 - 200$  kpc where positive detections are very rare for  $L^*$  galaxies but are common in the outer halos of the  $z \sim 2$  quasar hosts. These differences would be further accentuated if one scaled the impact parameters by estimates of the virial radii for these two populations ( $r_{\text{vir}}^{\text{QPQ}} \approx 160$  kpc,  $r_{\text{vir}}^{L^*} \approx 290$  kpc). We conclude, at very high confidence, that the halos of massive,  $z \sim 2$  galaxies contain a much greater reservoir of cool metals than modern  $L^*$  galaxies.

The figure also presents estimations of  $\langle W_{1334} \rangle$  for the COS-Dwarfs survey (Bordoloi et al. 2014, Bordoloi et al., in prep). These are based on 39 measurements of  $W_{1334}$

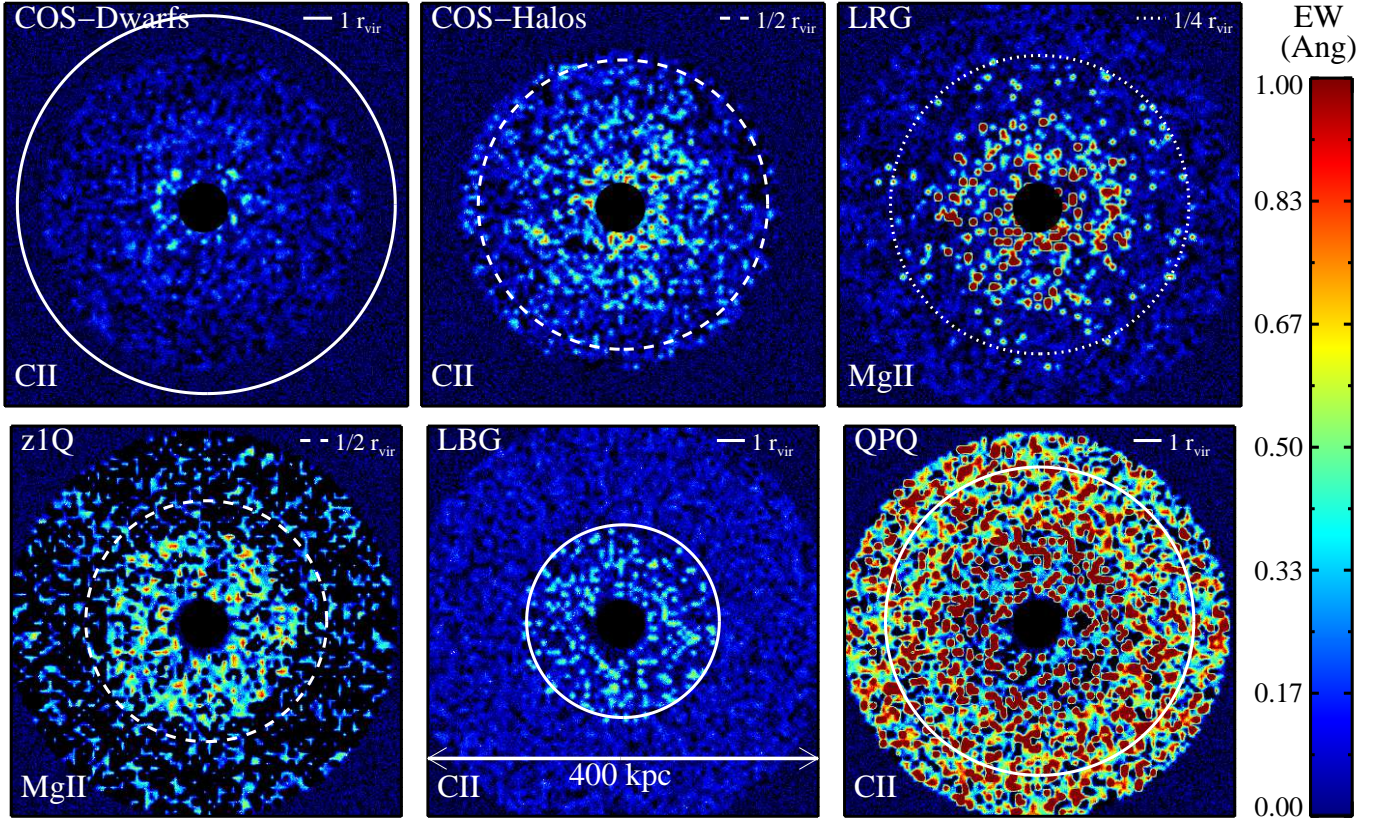


FIG. 11.— A visualization of the C II 1334 absorption measured statistically for  $z \sim 0$  luminous galaxies (COS-Halos; Werk et al. 2013),  $z \sim 2$  star-forming galaxies (LBGs), [LRGs], and the massive  $z \sim 2$  galaxies hosting quasars (QPQ; this paper). The color bar indicates the  $W_{1334}$  values in Å. Each cut-out is 400 kpc on a side and the solid (dotted/dashed) white circle indicates the estimated full (quarter/half) virial radius of each galaxy population. This exercise ignores the inner 20 kpc where the ISM of the galaxy may dominate and little data exists. The outer edges of the maps are also arbitrarily defined, i.e. not physical. The maps are constrained to give the observed distribution of  $W_{1334}$  and/or  $\langle W_{1334} \rangle$  values in several annuli but we emphasize that the size of the clumps (taken to be 5 kpc) and their distribution (taken to be random) need not hold in the real universe.

from  $L \lesssim 0.1L^*$  galaxies at  $z < 0.1$  drawn from the SDSS. The measured values are smaller still than the (nearly) coeval  $L^*$  galaxies, suggesting that the cool CGM depends on stellar/halo mass.

Figure 10 also presents estimations for the average equivalent widths of low-ion metals from the halos of  $z \sim 0.5$ , luminous red galaxies (LRGs). This estimate is derived from the measurements of Zhu et al. (2014, hereafter Z14) for the average equivalent widths of Mg II 2796,  $\langle W_{2796} \rangle$ . Because of their similar ionization potentials, we expect  $C^+$  to be roughly co-spatial with  $Mg^+$ -bearing gas.<sup>11</sup> Furthermore, we expect comparable equivalent widths for C II 1334 and Mg II 2796, especially when the transitions are both saturated. Empirically, the  $\approx 10$  systems from the COS-Halos dataset with strong detections<sup>12</sup> of both C II 1334 and Mg II 2796 show an average ratio of  $W_{2796}/W_{1334}=1.7$  (Werk et al. 2013). This scaling follows from the difference in rest wavelengths between the two transitions under the expectation that  $W_\lambda/\lambda$  is roughly constant. Therefore, we have scaled down the Z14 measurements accordingly to estimate  $\langle W_{1334} \rangle$  for the LRGs. Surprisingly,

the LRG results trace (at least roughly) the values for the  $L^*$  galaxies. This indicates that the massive halos of  $L \gg L^*$  galaxies contain substantial, cool and enriched gas at all epochs, independent of on-going star-formation in the central galaxy (as found for red-and-dead galaxies at  $z \sim 0.2$ ; Thom et al. 2012). This even includes galaxy clusters which exhibit an enhanced incidence of strong Mg II systems within  $r_{\text{vir}}$  ( $W_{2796} > 2\text{Å}$ ; Lopez et al. 2008; Andrews et al. 2013). Regarding our study of  $z \sim 2$  massive galaxies, the QPQ values systematically exceed the estimates for the LRGs at all impact parameters. Estimations of the covering fraction of Mg II absorption for LRGs also give much lower values than observed for the quasar hosts (Figure 10b). And, again, scaling by the virial radii would only further accentuate these differences ( $r_{\text{vir}}^{\text{LRG}} \approx 600$  kpc).

Pushing to  $z > 1$ , we compare our results against the coeval population of star-forming galaxies at  $z \sim 2$ , known as LBGs. Clustering analysis of the galaxies provides halo mass estimates of  $M_{\text{halo}} \lesssim 10^{12} M_\odot$  (Adelberger et al. 2005b; Bielby et al. 2013), i.e. a factor of three to five lower mass than the halos hosting luminous quasars. Figure 10 shows estimations for  $\langle W_{1334} \rangle$  and its covering fraction from the modest set of measurements in the literature (Adelberger et al. 2003, 2005a; Simcoe et al. 2006; Rudie et al. 2013; Crighton et al.

<sup>11</sup> Each element is ionized to this first state by  $h\nu < 1$  Ryd photons. One does note, however, that  $Mg^+$  has a significantly lower ionization potential than  $C^+$  (15.0 eV vs. 24.4 eV).

<sup>12</sup> Weaker Mg II 2796 systems show a nearly the same equivalent width as C II 1334 (Narayanan et al. 2008).

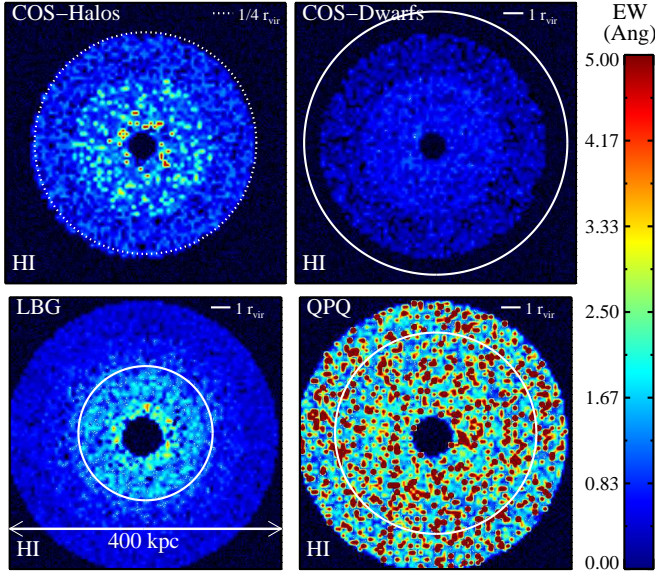


FIG. 12.— Visualization of the CGM in H I Ly $\alpha$  with rest-frame equivalent width given by the color bar (in  $\text{\AA}$ ; see Figure 11 caption and the text for details). The figure illustrates clearly the much higher incidence of strong H I Ly $\alpha$  absorption associated with the  $z \approx 2$  massive galaxies hosting quasars. This population marks the peak in the cool CGM. The inner/outer edges of the maps are arbitrarily defined by data coverage, i.e. not physical. The maps are constrained to give the observed distribution of  $W_{1334}$  and/or  $\langle W_{1334} \rangle$  values in several annuli but we emphasize that the size of the clumps (taken to be 5 kpc) and their distribution (taken to be random) need not hold in the real universe.

2013).<sup>13</sup> Consistent with the low covering fraction of optically thick gas reported by Rudie et al. (2013), the  $\langle W_{1334} \rangle$  and  $f_C$  values are small and significantly lower than the QPQ measurements. Even if we scale by the (likely) smaller virial radius for LBGs ( $r_{\text{vir}}^{\text{LBG}} \approx 100$  kpc), the massive galaxies hosting quasars exhibit far greater low-ion absorption on all scales within  $r_{\text{vir}}$ . Lastly, the figure shows recent results on the measurements of Mg II around  $z \sim 1$  quasars (z1Q; Farina et al. 2014). As with the LRGs, we scale these Mg II measurements down by a factor of 1.7 to compare them to the C II 1334 results. It is evident that the z1Q results lie between the QPQ and all other studies. This comparison indicates modest evolution in the strength and covering fraction of cool gas around galaxies hosting quasars, consistent with the expected mild evolution in the masses of halos hosting quasars with decreasing redshift (Richardson et al. 2012; Shen et al. 2013c).

To summarize the results of Figure 10, the CGM of massive galaxies hosting  $z \sim 2$  quasars exhibits a higher incidence and larger average equivalent widths of low-ion absorption than that measured for any other galaxy population at any epoch. Previously, we reached the same conclusion for H I Ly $\alpha$  absorption (QPQ5, QPQ6). We conclude that *the CGM of these massive  $z \sim 2$  galaxies represents the pinnacle of cool halo gas in the Universe.*

To further illustrate this primary result, we constructed “maps” of the CGM. For C II 1334 in QPQ, we average the  $W_{1334}$  measurements in several annuli for  $R_{\perp} \leq 200$  kpc. Within each annulus, we drew randomly from the observed  $W_{1334}$  distribution, assumed random

<sup>13</sup> We discuss results from the LBG stacked spectra of Steidel et al. (2010) in the following section.

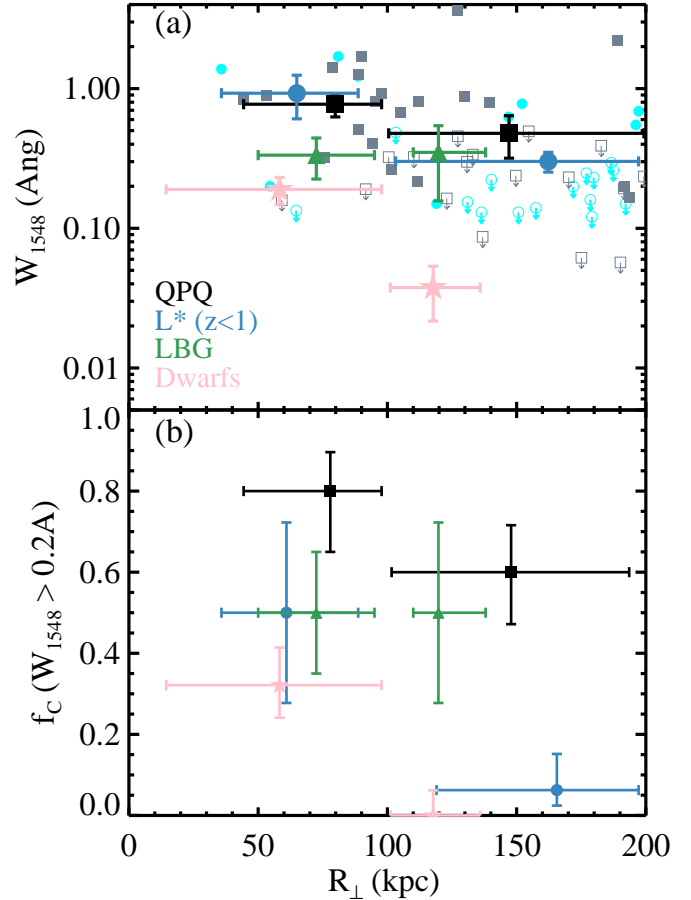


FIG. 13.— Same as Figure 10 but for the C IV 1548 transition. For the  $L^*$  galaxies at  $z < 1$ , we adopt the measurements of Borthakur et al. (2013) and Chen et al. (2001). The QPQ sample exhibits the highest rest-frame equivalent widths and covering fractions than any other galactic population, but the differences are smaller than those observed for lower ionization states.

gaussian noise with a deviate of  $50 \text{ m}\text{\AA}$ , and generated “clumps” with an arbitrary size of 5 kpc. These clumps were randomly placed within each annulus, constrained to give approximately the observed  $W_{1334}$  distribution of C II 1334 absorption including non-detections (i.e. reproducing the observed covering fraction). Explicitly, for the annulus  $R_{\perp} = [30., 100]$  kpc we inserted 1152 clumps with an  $W_{1334}$  distribution matching the 12 pairs from the QPQ sample at these impact parameters with an additional dispersion of  $40 \text{ m}\text{\AA}$ . We ignored the inner 25 kpc which our pairs do not sample and where the galactic ISM is expected to contribute/dominate. The maps are also arbitrarily cut at  $R_{\perp} \approx 200$  kpc or less (e.g. the COS-Halos and COS-Dwarfs samples extend to only  $\approx 150$  kpc).

Figure 11 shows the results in  $400 \times 400$  kpc cut-outs for the COS-Halos survey (Werk et al. 2013), the COS-Dwarfs survey (Bordoloi et al., in prep), the LRGs (Z14; see the Appendix for details), the  $z \sim 1$  quasars (z1Q; Farina et al. 2014), the LBGs, and our QPQ results. This exercise illustrates that the low-ion absorption from the CGM of massive,  $z \sim 2$  quasars is qualitatively stronger than that of any other galactic population. We have repeated this exercise for the H I Ly $\alpha$  measurements where available, as presented in Figure 12. For the LBGs, we take the average  $W_{\text{Ly}\alpha}$  values reported

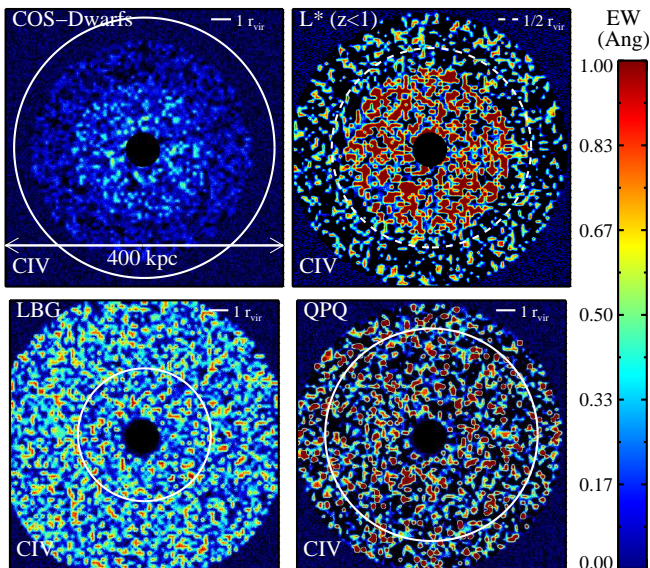


FIG. 14.— Illustrative map of the CGM in C IV 1548 absorption with equivalent width given by the color bar (in Å; see Figure 11 caption and the text for details). The figure illustrates a high incidence of strong C IV 1548 in all populations except the dwarf galaxies.

by Steidel et al. (2010) and Rakic et al. (2012), assuming a 50% scatter, and a unit covering fraction. All of these equivalent widths were corrected for absorption by the background IGM. The results further emphasize that cool gas absorption is systematically larger for the QPQ dataset on all physical scales and also when considered as a fraction of the virial radius. At the same time, the CGM of the  $L^*$  galaxies at  $z \sim 0$  is qualitatively similar to the LBGs (the latter is stronger when scaled by  $r_{\text{vir}}$ ).

To complete the comparisons, we present results on C IV 1548 where available (Figures 13, 14). Similar to the transitions known to trace the cool CGM (H I Ly $\alpha$ , Mg II, C II), the C IV absorption strength for QPQ exceeds that for all of the  $z < 1$  populations. One notes, however, that the LBG measurements more closely follow those of the  $z \sim 2$  quasar hosts. The differences between the populations are far more apparent in the C II 1334 and H I gas, implying that C IV 1548 (which likely traces a more highly-ionized and possibly warmer gas) may be associated to a medium that is less sensitive to the underlying halo mass.

We may also compare mass estimates for the cool CGM metals around these galaxies with our own QPQ estimates, as presented in Figure 9. We remind the reader that these estimates are strictly lower limits. Overplotted on the QPQ result is an estimate for the cumulative mass in metals traced by Mg II absorption in the halos of LRGs (Z14). The curve shows the best-fit halo model from their analysis, where we have assumed that Mg represents 6% of the total metal mass (as in the Sun) and no correction for ionization, but note that Z14 did impose a modest correction for line-saturation. The figure also shows the cumulative mass profile from the COS-Halos sample ( $z \sim 0$ ,  $L^*$  galaxies) generated in the same manner as the QPQ data (their survey, however, only probes to  $R_{\perp} \approx r_{\text{vir}}/2$ ). Remarkably, the COS-Halos and LRG profiles are very similar, suggesting a similar mass in cool gas within  $r_{\text{vir}}$  despite the order-

of-magnitude difference in their halo masses (although formally these estimates are lower limits). These curves intersect the profile for the  $z \sim 2$  massive galaxies<sup>14</sup>, but the latter rises to a value several times larger than that derived for LRGs at  $r_{\text{vir}}$ . And, we emphasize that a majority of the metal mass in the halos of LRGs occurs at  $R_{\perp} > 250$  kpc where satellite galaxies may dominate, as suggested by the low covering fraction of strong Mg II absorption at such impact parameters (Bowen & Chelouche 2011; Gauthier & Chen 2011, see also the Appendix).

The figure also shows the total, cumulative metal mass estimated for the cool CGM of  $L^*$  galaxies, taken from the analysis of Werk et al. (2014, see also Peebles et al. 2014). Specifically, we scaled their estimate for the surface density profile of silicon (their Equation 6) by assuming silicon represents 7% of the total mass in metals. Unlike the mass estimations that we provided first (solid curves), the Werk et al. (2014) analysis includes significant ionization corrections based on their detailed modeling of the absorption lines and line-saturation has a more modest effect. For  $R_{\perp} > 0.55r_{\text{vir}}$ , we have extrapolated their best-fit and show that curve as a dotted line. This mass profile exceeds the QPQ profile based on our simple and highly conservative prescription (solid black line). The more realistic estimate for the QPQ mass profile (dashed black line), however, exceeds the values for  $L^*$  galaxies at  $z \sim 0$ . These results further supports the conclusion that the cool CGM of galaxies peaks in  $z \sim 2$ , massive galaxies which host luminous quasars. In § 5.5, we speculate on possible physical explanations.

### 5.3. The Incidence of Strong Mg II Absorption

The concept that the cool CGM peaks at  $z \sim 2$  was previously suggested from analysis on the incidence of strong Mg II systems  $\ell(X)_{\text{MgII}}$  (Prochter et al. 2006; Ménard et al. 2011; Matejek & Simcoe 2012). These authors emphasized that the redshift evolution of  $\ell(X)_{\text{MgII}}$  with redshift tracks the cosmic star formation history (SFH) of the universe. We discuss connections between SF and the CGM in the following sub-section, but consider here the contribution of massive  $z \sim 2$  galaxies to the strong Mg II absorbers.

To perform the comparison, we must first estimate the covering fraction of strong Mg II absorption around quasar halos. Unfortunately, our dataset provides only a small sample of pairs where we can analyze Mg II 2796 directly. An alternate approach is to adopt the  $f_C = 70\%$  covering fraction of strong C II 1334 absorption ( $W_{1334} > 0.2\text{Å}$ ) and scale this equivalent width limit by 1.7 (see the previous section). We conservatively adopt  $f_C = 0.7$  to  $R_{\perp} = 200$  kpc for  $W_{2796} \geq 0.3\text{Å}$ . Our sample does include 13 pairs with  $R_{\perp} < 200$  kpc and good spectral coverage of Mg II 2796. As expected, all of the systems with strong C II 1334 absorption also exhibit strong Mg II 2796 absorption. Of the 13 pairs, five have  $W_{2796} > 1\text{Å}$  for a covering fraction of  $0.4 \pm 0.1$ . For the following we conservatively assume that these massive galaxies have  $f_C^{\text{MgII}}(> 1\text{Å}) = 0.3$  to  $R_{\perp} = 200$  kpc.

The incidence of Mg II absorption that one ascribes to the CGM of galaxies scales with their comoving number

<sup>14</sup> These begin at  $R_{\perp}/r_{\text{vir}} \approx 0.3$  because of the lack of sightlines that probe smaller scales.

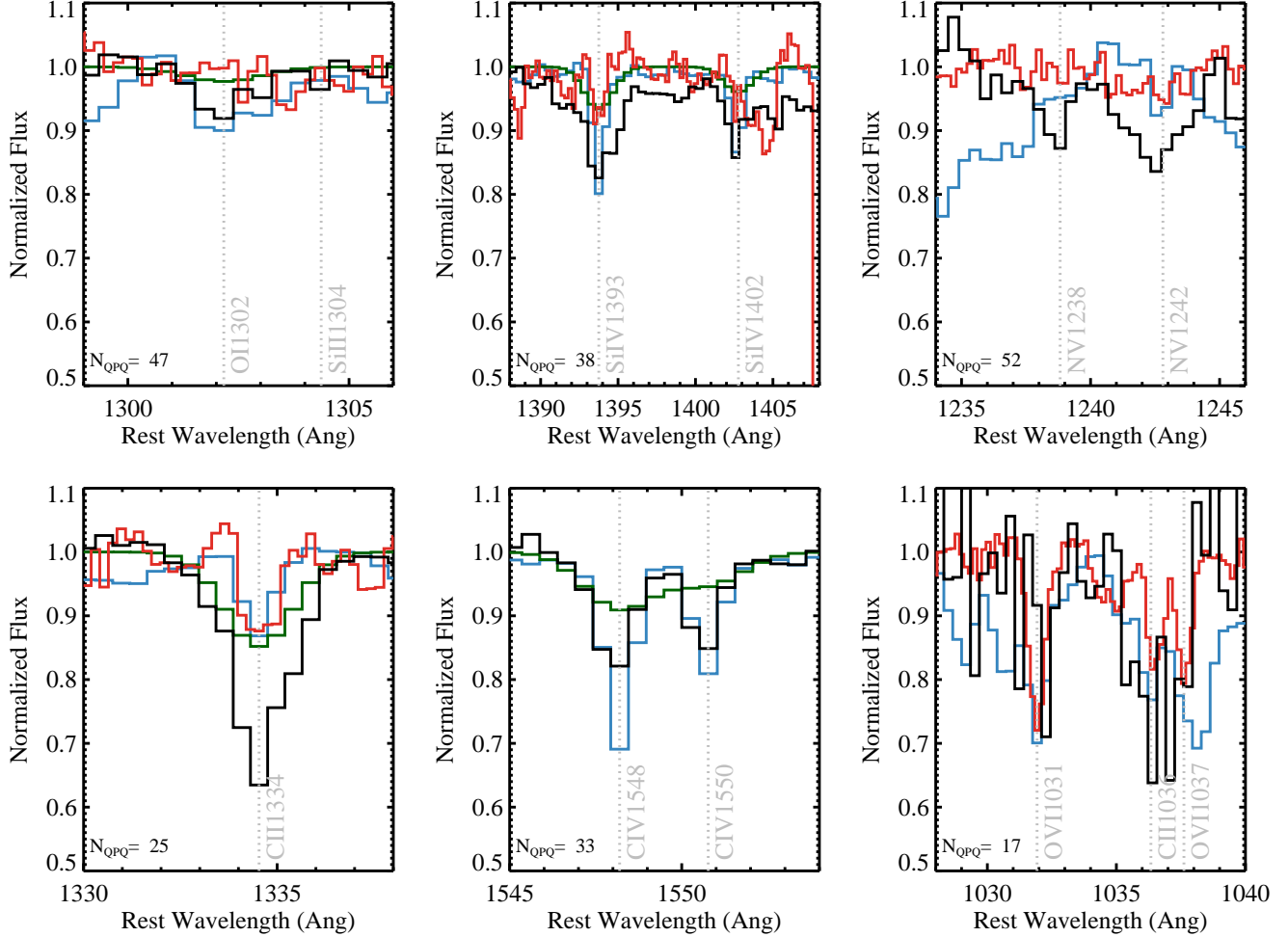


FIG. 15.— Stacked spectra for a series of low and high-ion metal transitions tracing the CGM of galaxies across cosmic time: QPQ (black; this program),  $z \sim 2$  LBGs (green; Steidel et al. 2010),  $z \sim 0$   $L^*$  galaxies (red; Werk et al. 2013), and a set of LLS at  $z \sim 3$  with  $N_{\text{HI}} < 10^{17.5-19} \text{ cm}^{-2}$  (cyan; Fumagalli et al. 2013). It is evident that the  $z \sim 2$  massive galaxies hosting quasars exhibit the strongest metal-line absorption at  $R_{\perp} < 200$  kpc of any galactic population. There are indications of N V and O VI absorption in the QPQ dataset, although these profiles are significantly affected by coincident IGM absorption. The profiles from QPQ are relatively similar to that observed in the  $z \sim 3$  LLS, suggesting the latter trace a similar CGM.

density  $n_{\text{com}}^{\text{QPQ}}$  and the projected effective area of absorption from the CGM (Bahcall & Peebles 1969),

$$\ell(X)_{\text{MgII}} = \frac{c}{H_0} n_{\text{com}}^{\text{QPQ}} f_C^{\text{MgII}} \pi R_{\text{max}}^2. \quad (1)$$

A very conservative estimate for  $n_{\text{com}}^{\text{QPQ}}$  is to adopt the number density of luminous quasars ( $10^{-5} \text{ Mpc}^{-3}$ ; Hopkins et al. 2007), giving  $\ell(X)_{\text{MgII}} = 0.0016$  for  $W_{2796} > 1 \text{ \AA}$ . Because the duty cycle of quasar activity is believed to be short ( $10^{-3}$ ), this is a very conservative limit. If we instead assume that the CGM profiles of massive galaxies are independent of whether a quasar is shining<sup>15</sup>, a more reasonable estimate for  $n_{\text{com}}^{\text{QPQ}}$  is the number density of halos with mass consistent with the observed clustering, i.e.  $M_{\text{halo}} \sim 10^{12.5} M_{\odot}$  (White et al. 2012). Here we adopt a minimum mass  $M_{\text{min}}^{\text{QPQ}} = 10^{12} M_{\odot}$  giving  $n_{\text{com}}^{\text{QPQ}}(M_{\text{halo}} > M_{\text{min}}^{\text{QPQ}}) = 7 \times 10^{-4} \text{ Mpc}^{-3}$  at

<sup>15</sup> We also stress that the radiation field from the quasar is very likely to *reduce* the covering fraction by ionizing Mg to a higher ionization state than  $\text{Mg}^+$ .

$z = 2.5$ , and emphasize that this number density has a steep dependence on  $M_{\text{min}}^{\text{QPQ}}$ . Altogether, we recover  $\ell(X)_{\text{MgII}}^{\text{QPQ}}(> 0.3 \text{ \AA}) = 0.25$  and  $\ell(X)_{\text{MgII}}^{\text{QPQ}}(> 1 \text{ \AA}) = 0.11$ . The observed incidence of strong Mg II systems at  $z \gtrsim 2$  has been measured along quasar sightlines to be:  $\ell(X)_{\text{MgII}}^{\text{IGM}}(> 0.3 \text{ \AA}) = 0.27$  and  $\ell(X)_{\text{MgII}}^{\text{IGM}}(> 1 \text{ \AA}) = 0.11$  (Nestor et al. 2005; Prochter et al. 2006; Matejek & Simcoe 2012; Seyffert et al. 2013). We conclude that a significant fraction and very possibly the overwhelming majority of strong Mg II systems at  $z \sim 2$  occur within the halos of massive galaxies.

One test of this conclusion is to search for the galactic counterparts of strong Mg II systems at  $z = 2$ . Bouché et al. (2012) have performed a survey of 20 Mg II systems with  $W_{2796} \gtrsim 2 \text{ \AA}$  at  $z \approx 2$  using integral field unit (IFU) spectroscopy tuned to the  $\text{H}\alpha$  emission line. They report an unobscured-SFR sensitivity limit of  $\approx 3 M_{\odot} \text{ yr}^{-1}$  and find only 4 galaxy counterparts within their  $\approx 40 \text{ kpc}$  search radius. At first glance their results appear inconsistent with our assertion that strong Mg II absorption is dominated by massive halos, whose

SFRs we expect to exceed  $5M_{\odot}\text{yr}^{-1}$ . We stress, however, that the cross-section is dominated by large impact parameters, i.e. at  $R_{\perp} > 40\text{ kpc}$  which exceeds their IFU field-of-view. Therefore, we encourage a similar search for galaxy counterparts to larger impact parameters.

Before concluding this sub-section, we also note that one recovers a similar estimate for  $\ell(X)_{\text{MgII}}$  from the CGM of  $z \sim 1$  quasars where Farina et al. (2014) measure  $f_C(W_{2796} > 0.6\text{ \AA}) \approx 0.2$  to  $R_{\perp} = 200\text{ kpc}$ . Quasar clustering at  $z \approx 1$  implies a halo mass of  $\approx 4 \times 10^{12}h^{-1}M_{\odot}$  (Richardson et al. 2012; Shen et al. 2013c). Therefore, we adopt  $M_{\text{min}}^{\text{z1Q}} = 10^{12}M_{\odot}$  and calculate  $n_{\text{com}}^{\text{z1Q}}(M > M_{\text{min}}^{\text{z1Q}}) = 1.5 \times 10^{-3}\text{ Mpc}^{-3}$  at  $z = 1$ . Altogether, this gives  $\ell(X)_{\text{MgII}}^{\text{z1Q}} = 0.16$  which is an appreciable fraction ( $\sim 70\%$ ) of the incidence observed along quasar sightlines:  $\ell_{\text{MgII}}^{\text{IGM}}(X; z = 1, W_{2796} \geq 0.6\text{ \AA}) = 0.22$  (Seyffert et al. 2013).

#### 5.4. Insights from Stacked Spectra

In Figures 3 and 4 (§3), we presented the averaged C II 1334 and C IV 1548 profiles as a function of pair separation. These stacked profiles illustrated the results apparent in the individual measurements: a high incidence of strong C II 1334 absorption at  $R_{\perp} < 200\text{ kpc}$ , the steep decline beyond, and the sustained incidence of strong C IV absorption to  $R_{\perp} \approx 1\text{ Mpc}$ . We now extend this exercise to additional transitions and offer qualitative comparison to stacked spectra generated from other CGM datasets. Our primary interests are to assess additional ionization states and to further accentuate aspects of the CGM relative to other galaxy populations. We restrict all of the following analysis and discussion to  $R_{\perp} < 200\text{ kpc}$ .

We have generated stacked QPQ spectra at four additional transitions – O I 1302, N V 1238, Si IV 1393, and O VI 1031 – permitting an assessment of those and a few additional, neighboring transitions. Except for Si IV, these new stacks include spectral regions within the Ly $\alpha$  forest of the b/g quasar and therefore are significantly contaminated by the coincident  $z \sim 2$  IGM. With sufficient sample size, the IGM does average down to a relatively smooth effective opacity (QPQ6 Becker et al. 2013), but for the bluest transitions considered here the sample is small (several tens of pairs) and both Ly $\beta$  and Ly $\alpha$  opacity contributes. These data are compromised by the IGM.

Aside from Si IV, we utilize the same algorithm employed in QPQ6 for continuum estimation in the Ly $\alpha$  forest and to stack the data at the transitions of interest. Each pair has equal weighting and each spectrum was resampled to  $\Delta v = 100\text{ km s}^{-1}$  pixels centered on the transition before performing a straight average. We have also normalized each stacked spectrum to give approximately unit flux at large offsets from the expected transitions. The results are presented in Figure 15.

The spectra exhibit strong detections of the Si IV doublet and weak but significant absorption at O I 1302. The Si II 1304 transition is not positively detected which is somewhat surprising given the detection of Si II 1526 in the C IV 1548 stacks (Figure 4). We attribute this to systematics from IGM absorption in the Si II 1304 profile and a significantly poorer S/N. Meanwhile, the N V

and especially the O VI doublets suffer from stochastic variations in the IGM absorption. The data suggest positive detections but we only set generous upper limits to the average equivalent widths of  $W_{1238} < 0.2\text{ \AA}$  and  $W_{1031} < 0.5\text{ \AA}$ .<sup>16</sup> One will require higher spatial resolution and/or a much larger dataset to more effectively probe this highly ionized gas.

Overplotted on these data are the average absorption-line profiles for 20 LLS with  $\tau > 2$  taken from the  $z \sim 3$  survey of optically thick gas by Fumagalli et al. (2013). We have restricted their sample to systems without strong damping at H I Ly $\alpha$ <sup>17</sup>, corresponding to  $N_{\text{HI}} \lesssim 10^{20}\text{ cm}^{-2}$ , because very few of the QPQ sightlines exhibit such high H I column densities (QPQ6). We have also smoothed stacks of their MagE spectra by 4 pixels and resampled to  $50\text{ km s}^{-1}$  pixels. With the exception of C II 1334, where the QPQ sample shows stronger absorption, the sets of stacked profiles from QPQ and these LLS are qualitatively similar. This suggests that the CGM of massive galaxies is a major contributor to at least the set of strong metal absorption systems in the LLS cohort. We reached a similar conclusion in QPQ6 based on the high covering factor and an estimated abundance for the halos hosting quasars.

Figure 15 also shows pseudo-spectra for the CGM surrounding LBGs using the results of Steidel et al. (2010). These were generated by averaging the reported equivalent widths from their stacked spectra for the  $R_{\perp} \approx 63$  and  $103\text{ kpc}$  bins (their Table 4) and representing the profiles as Gaussians with  $\sigma = 200\text{ km s}^{-1}$ .<sup>18</sup> Consistent with the results for the individual measurements of C II 1334 (Figure 10; QPQ5) and H I Ly $\alpha$  (QPQ6), the absorption strength of LBGs for  $R_{\perp} < 120\text{ kpc}$  is weaker than the average absorption observed for the halos hosting quasars averaged over  $R_{\perp} \leq 200\text{ kpc}$ . This includes both the low and high-ionization species. These stacked spectra confirm that the CGM of the massive galaxies hosting quasars exceeds that of the coeval, star-forming LBG population.

Lastly, we include a set of stacked profiles from the COS-Halos survey, generated with the same QPQ algorithms but sampled with  $50\text{ km s}^{-1}$  pixels. The COS-Halos sample includes all 44 galaxies studied in Werk et al. (2013). Consistent with Figure 10, the average C II 1334 absorption is significantly stronger in the CGM of massive  $z \sim 2$  galaxies. Similarly, the COS-Halos sightlines exhibit negligible absorption from the other low-ion transitions. In fact, the absorption in the  $z \sim 0$  CGM of  $L^*$  galaxies is dominated by intermediate ions (C<sup>++</sup>, Si<sup>++</sup>; not shown here) and O VI, in addition to the H I Lyman series (Tumlinson et al. 2011; Werk et al. 2013; Tumlinson et al. 2013).

To summarize, the average profiles of the QPQ sample exhibit metal absorption with systematically larger equivalent widths than any other CGM, especially for

<sup>16</sup> Taking all of the QPQ7 sightlines that cover N V (i.e. to  $R_{\perp} = 1\text{ Mpc}$ ), the stacks suffer much less from IGM stochasticity and we measure  $W_{1238} < 0.1\text{ \AA}$ .

<sup>17</sup> Including the LLS with larger  $N_{\text{HI}}$  values increases the average absorption, especially O I 1302.

<sup>18</sup> We have digitized their Figures 17-20 and confirm that our pseudo-spectra are a reasonable match to the data when compared at the same spectral resolution.

the lower ionization states. These stacks more resemble, at least qualitatively, the profiles exhibited by strong LLS at similar redshift suggesting a significant fraction of the LLS may be associated to massive halos (see also QPQ6).

### 5.5. Inferences on the Cool CGM

The results presented in the previous sub-sections demonstrate that the gas surrounding massive,  $z \sim 2$  galaxies hosting quasars represents the pinnacle of the cool CGM. In terms of the strength of H I and low-ion metal absorption, the radial extent – physical and scaled to  $r_{\text{vir}}$  – of this cool gas, and the estimated metal mass, the CGM of the QPQ sample represents the greatest reservoir of cool gas. We now explore and speculate on the conditions that favor the growth of this massive reservoir in this environment and at this epoch.

Fundamentally, there are two factors that set properties of the cool CGM: (1) the total mass in gas and metals within the galactic halo; and (2) the fraction of this medium that is in a cool phase ( $T \sim 10^4$  K). The first factor, we believe, is set by the mass of the dark matter halo; the baryonic mass scales with dark matter and, presumably, the metal mass tracks the stellar mass which is also proportional to halo mass (e.g. Mandelbaum et al. 2005; Moster et al. 2010). The second aspect – cool gas fraction – is determined by a complex set of competing physical processes: the flow of cool gas into/out of galaxies (processes that strip the ISM from galaxies, accretion of cool material from the IGM), shock heating, cooling of warm gas in the halo, interactions of the cold phase with the predicted hot phase, via processes like conduction, turbulent mixing/ablation, etc. We begin by considering several of these processes and argue that individually they are sub-dominant to the halo-mass dependence.

Is the cool CGM driven by quasar feedback? Given that the QPQ experiment uses quasars as signposts for the locations of massive galaxies, one might speculate that the AGN directly impacts the results, especially since quasar activity peaks at  $z \sim 2-3$ . We also note that both samples probing quasars, ours and the experiment at  $z \sim 1$  (Farina et al. 2014) recover the two dominant populations regarding the cool CGM. Indeed, quasar feedback is frequently invoked as an effective means to transport cool, dense gas from the ISM of galaxies (e.g. Silk & Rees 1998; Sijacki et al. 2007; Choi et al. 2014). Furthermore, we have identified examples in our own QPQ survey of extreme kinematics suggestive of non-gravitational flows (QPQ3). Such systems are relatively rare, however, and are not uniquely explained by quasar feedback (QPQ3, QPQ8).

While quasars undoubtedly play a role in the galaxy formation process, the body of data presented in the previous sub-sections (Figures 9-10) indicates that the AGN itself has a minor role in producing the cool CGM. First, and most obvious, we recognize that many galaxy populations exhibit a substantial cool CGM without a quasar (e.g. Figure 10); an active galactic nucleus is not required. Second, as regards the QPQ measurements, our results indicate substantial mass in H I and metals to at least 200 kpc. Even if quasars are active for  $10^8$  yr and accelerate material to  $500 \text{ km s}^{-1}$ , this gas would only reach 50 kpc upon the termination of that quasar cycle. One would need to invoke multiple quasar episodes to reach 200 kpc. Third, we question whether quasar

feedback could expel the total mass inferred (nearly that of an entire ISM) and provide a nearly unit covering fraction of cool material (QPQ3, QPQ6; Figure 9). Fourth, quasars are more likely to *suppress* the presence of cool halo gas because their ionizing radiation field easily over-ionizes gas to very large distances ( $\sim 1$  Mpc; e.g. QPQ2, Chelouche et al. 2008). While we have argued that quasars emit their radiation anisotropically, we still expect suppression within the nearby environment. Fifth, while kpc-scale jets from radio-loud quasars could play a role, only a small fraction of quasars exhibit such emission ( $\sim 10\%$  Ivezić et al. 2002). Sixth, some models for triggering quasar activity envision galaxy-galaxy mergers are required to funnel gas to the galaxy centers. While this could enhance the incidence of cool gas on scales of tens kpc, we question whether such interactions would influence the CGM at  $R_{\perp} > 100$  kpc. We conclude that at most, quasar episodes help shape the nature of the CGM but that they do not define it.

Is the cool CGM generated from flows driven by star-formation feedback, i.e. the outflow of cool gas from the ISM? The presence of heavy elements within the CGM has led many researchers to link this gas to processes of star-formation feedback (e.g. Adelberger et al. 2005a; Oppenheimer & Davé 2006; Steidel et al. 2010; Ménard et al. 2011; Stinson et al. 2012; Shen et al. 2013b). Figure 9 emphasizes the nearly ubiquitous presence of metals, indicating a fraction of the observed medium has previously cycled through a galaxy and has then been transported into the halo. Such associations are supported by the observation of cool gaseous outflows from star-forming galaxies across cosmic time (e.g. Pettini et al. 1998; Martin 2005; Weiner et al. 2009; Rubin et al. 2013). One notes further that  $z \sim 2$  corresponds to the approximate peak in the cosmic star-formation history (SFH). Perhaps this explains the remarkable CGM of our  $z \sim 2$  massive galaxies, i.e. one could associate the peak in SF to a peak in the cool CGM. By the same token, of course, a peak in the cool CGM of galaxies may drive (i.e. fuel) a peak in SF activity. So, is it the chicken or the egg? Perhaps it is neither but both. To maintain even a modest SFR for Gyrs, one requires a fresh fuel supply and, in turn, SF feedback enriches the surrounding medium. In this regard, elevated SF may be a natural outcome of a massive, cool CGM and vice-versa.

Turning to the results presented here, the majority of galaxies known to exhibit a cool CGM also are actively forming stars and, presumably, supernovae with associated feedback.<sup>19</sup> This is not universal, however. The obvious exceptions are the LRGs whose large covering fraction to strong Mg II absorption at small  $R_{\perp}$  indicates gas related to the central galaxy (Figure 11; Bowen & Chelouche 2011, Z14). Furthermore, a cool CGM is also present in the halos of present-day, red-and-dead galaxies (Thom et al. 2012). Furthermore, within the star-forming population, there is little dependence of the strength of absorption on SFR or specific SFR. For example, Figure 10 demonstrates that the present-day  $L^*$  galaxies and  $z \sim 2$  LBGs have CGM with similar

<sup>19</sup> Currently, there is no galaxy population without a cool CGM, although such gas appears suppressed in the cluster environment (Yoon & Putman 2013, but see Lopez et al. (2008)).

characteristics (see also Chen 2012). Both populations have comparable halo mass, yet an order-of-magnitude difference in active SFR. Similarly, the galaxies hosting quasars do not exhibit evidence for elevated SFRs but instead lay along the so-called “main sequence” of SF at  $z \sim 2$  (Rosario et al. 2013). Lastly, the excess in cool gas extends to many hundreds kpc, i.e. too great a distance to be directly influenced by the host galaxy. We conclude that the instantaneous SFR is unrelated to the current properties of the cool CGM. While SF feedback is an absolutely critical ingredient to enriching the cool CGM, we suspect its integrated impact only contributes over long time-scales. More likely, the presence of a cool CGM is a prerequisite – but not a necessary condition – for active SF.

Is the cool CGM driven by the accretion of fresh, cool material from the IGM (i.e. “cold flows” or “streams”)? Several lines of argument disfavor this scenario. First, the CGM gas is significantly enriched, at all epochs. Metal enrichment by the first stars and/or low mass galaxies infalling with the streams undoubtedly generate some metals (e.g. Madau et al. 2001; Shen et al. 2011), but current models predict lower metallicity flows ( $\approx 1/100$  solar; Fumagalli et al. 2011b; van de Voort & Schaye 2012; Shen et al. 2013b) than observed in the CGM (with important exceptions; Ribaudo et al. 2011; Fumagalli et al. 2011a). Second, cosmological simulations predict that present-day  $L^*$  galaxies have ceased to accrete dark matter (Diemand et al. 2007; Diemer et al. 2013). Therefore, the cool CGM of modern galaxies is unlikely to arise primarily from ongoing cold gas accretion. Third, none of the existing models predict a covering fraction of cool gas comparable to that observed in the massive galaxies hosting  $z \sim 2$  quasars (QPQ6; Fumagalli et al. 2014). In short, we conclude that cold accretion alone cannot reproduce the observed cool CGM. We may speculate, however, that the extreme CGM exhibited by massive  $z \sim 2$  galaxies does indicate a contribution from the elevated accretion of cool gas onto these halos. Indeed, a supply of cool H I gas may be required to fuel star-formation in these massive galaxies and, especially, the extreme examples among the population (sub-mm galaxies). Given the properties of the CGM illustrated in this manuscript, one may speculate whether the galaxies hosting quasars are poised to undergo a major burst of SF. We return to this point in § 5.7.

In lieu of quasar activity, SF feedback, cold accretion and any other astrophysical mechanism<sup>20</sup> as the obvious dominant factor for the cool CGM, we posit that its properties are most fundamentally driven by the halo mass. This conclusion follows from several of the comparisons presented in the previous subsections (Figures 10-15). Consider first the results for LBGs against those for the  $z \sim 2$  massive galaxies hosting quasars. Aside from the luminous quasar (discussed above), these coeval galaxy populations differ primarily in one characteristic: halo mass, by a factor of  $\approx 3 - 5$ . The SFRs estimated from far-IR observations of galaxies hosting quasars indicate they lie along the “main-

sequence” of star-formation at  $z \sim 2$  (Rosario et al. 2013). Owing to the higher halo mass of these systems, the SFR may be higher than the LBGs but the dependence on mass is modest ( $\text{SFR} \propto M_*^{0.57}$ ; Whitaker et al. 2012). The difference in halo mass, meanwhile, is well established through the clustering strength of LBGs and quasars (Adelberger et al. 2005a; White et al. 2012). It is further confirmed by the difference in H I absorption strength on large scales (QPQ6, Rakic et al. 2012, 2013; Font-Ribera et al. 2013). Excess H I absorption extends down to the smallest scales probed in each sample, i.e. well within the dark matter halos. And the same holds for every other ion examined in both populations (Figure 15). We conclude that the distinct CGM properties are manifested by the difference in halo mass.

The dominant role of halo mass is further supported through comparison of the nearly coeval,  $z \sim 0$   $L^*$  and dwarf galaxies. One finds that the latter exhibit a much weaker, cool CGM (e.g. Figure 10). This holds despite the fact that the latter are predicted to have expelled a much higher fraction of metals and gas from their central galaxy (e.g. Shen et al. 2013a). In addition, comparing the cool CGM of the  $L^*$  galaxies at  $z \sim 0$  with  $z \sim 2$  LBGs one observes very similar CGM properties despite substantial differences in the active SFR and SFH. Their halo and stellar masses, however, are comparable. Lastly, studies that associate Mg II absorption to galaxies suggest a scaling in absorption strength with halo mass (Chen et al. 2010b; Churchill et al. 2013). Therefore, we conclude that *halo mass is the dominant factor in establishing the properties of the cool CGM*.

This final conclusion poses an immediate question: What about the LRGs which are the most massive halos and galaxies considered? Despite an order-of-magnitude higher halo mass, the absorption strength and estimated metal masses for the cool CGM of LRGs do not greatly exceed (or even match) that observed in the lower mass halos of  $z \sim 0$ ,  $L^*$  galaxies, the LBGs, and quasar hosts. This result is very unlikely to reflect lower gas and metal masses within the LRG halos. Indeed, X-ray observations of small galaxy groups with virial temperatures characteristic of the halos of LRGs ( $kT \sim 1\text{keV}$ ) exhibit a metal mass in Fe *alone* that exceeds  $10^9 M_\odot$  (Sasaki et al. 2014). Therefore, the cool gas around LRGs likely represents a tiny fraction of the total gas and metal budget within their dark matter halos. One draws similar conclusions for the cool gas related to the ICM of modern galaxy clusters (Lopez et al. 2008; Yoon & Putman 2013). Within these most massive halos, the cool CGM must be suppressed. An obvious explanation is that the plasma is too hot to support a major reservoir of cool gas. In fact, it is very possible that nearly all of the cool gas detected in the outer regions of these massive halos is related to material recently stripped from or within satellite galaxies (see also Appendix B).

So is halo mass the only factor? Certainly not. Better stated, what astrophysical processes that scale with halo mass most influence the cool CGM? One aspect must be the greater production of metals, i.e. a higher stellar mass within higher mass halos yields a higher output of metals. Only a fraction of these metals, however, are dispersed within the halo and it is possible that a smaller

<sup>20</sup> We add that tidal disruption of satellite galaxies is very unlikely to generate the entirety of the observed CGM but may certainly contribute.

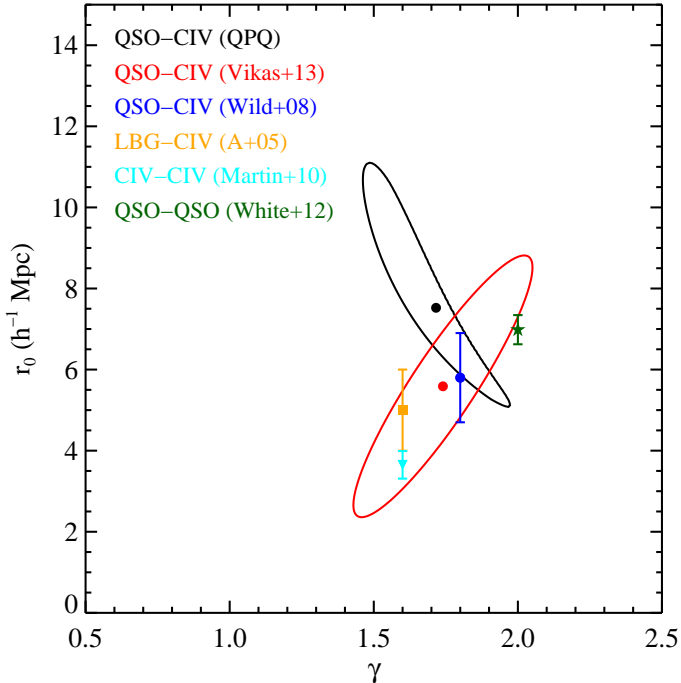


FIG. 16.— Comparison of constraints on the two-point quasar-quasar (green; White et al. 2012), C IV-C IV (cyan; Martin et al. 2010b), and quasar-C IV (blue, black, red; this paper, Vikas et al. 2013; Wild et al. 2008) cross-correlation functions. The latter exhibit good agreement at  $r_0 \approx 6h^{-1}$  Mpc and  $\gamma \approx 1.8$ . We also present the LBG-C IV cross-correlation function Adelberger et al. (2005b) for  $N_{\text{CIV}} \geq 10^{12} \text{ cm}^{-2}$  (yellow).

fraction is output for higher mass galaxies given their larger potential wells. We suspect, therefore, that another astrophysical factor is required. We propose that the principal factor is the characteristic density of halo gas  $n_{\text{halo}}$ . The neutral fraction is sensitive to  $n_{\text{halo}}^2$  via recombination and there may be additional non-linear effects, e.g. the self-shielding of ionizing radiation, higher cooling rates, a greater probability for instabilities that generate cool clouds. One further expects that for a given mass halo that  $n_{\text{halo}}$  is higher at higher redshift because the universe has a higher mean density. In fact, with the QPQ (and to a lesser extent zQ1) samples, we may have all of the astrophysical processes that contribute to the CGM working together to yield the observed pinnacle of the CGM.

### 5.6. The Clustering of C IV

In § 4.2, we presented analysis on the clustering of strong ( $W_{1548} > 0.3\text{\AA}$ ) C IV absorption with quasars, as estimated from the projected cross-correlation on scales  $R_{\perp}^{\text{com}} < 3h^{-1}$  Mpc. Our observations are well-described by a power-law, cross-correlation function  $\xi_{\text{CIV-Q}}(r) = (r/r_0)^{-\gamma}$  with  $r_0 = 7.5_{-1.4}^{+2.8} h^{-1}$  Mpc and  $\gamma = 1.7_{-0.2}^{+0.1}$  (Figures 6, 7). The large clustering amplitude, comparable to that measured from quasar clustering, implies that the C IV gas traces the same large-scale over-densities as the halos manifesting  $z \sim 2$  quasars. We now explore further the implications of this result.

Previous studies have examined the clustering of C IV gas with quasars on larger scales ( $R_{\perp}^{\text{com}} > 10h^{-1}$  Mpc; Wild et al. 2008; Vikas et al. 2013), the cluster-

ing with LBGs on comparable scales to our experiment (Adelberger et al. 2005a; Cooke et al. 2006), and also the C IV auto-correlation function (Quashnock & vanden Berk 1998; Martin et al. 2010b). All have reported significant clustering amplitudes, as summarized in Figure 16. These results have been interpreted as evidence that the C IV gas is physically associated to galaxies, i.e. the C IV gas resides within the dark matter halos of galaxies whose clustering amplitude scales with mass. Indeed, Vikas et al. (2013) estimated that strong C IV ( $W_{1548} > 1\text{\AA}$ ) at  $z \sim 2.5$  occurs primarily within galaxies hosted by dark matter halos with  $M_{\text{halo}} > 10^{12} M_{\odot}$ . This estimate follows from the cosmological paradigm which predicts that baryons trace the gravitational potential generated by dark matter and may be related to the latter in the regime of linear bias by a bias factor  $b$ ,  $\xi(r) = b^2 \xi_{\text{DM}}(r)$  (e.g. Davis & Peebles 1977; Scherrer & Weinberg 1998), which is usually valid at large scales  $\gg 1$  Mpc (but see Tejos et al. 2014). When combined with independent estimates of the quasar auto-correlation function, one may assess the bias factor and estimate the halo mass. Our results on the quasar-C IV clustering, obtained on smaller (and presumably non-linear) scales serve to confirm the Vikas et al. (2013) inferences. The results imply that the C IV absorption associated to quasars is characteristic of all massive halos.

One may also gain insight into the nature of absorption-line systems through comparisons of the cross-correlation functions with quasars. Taking the results presented here on C IV and those from QPQ6, we have (in order):  $r_0^{\text{DLA}} = 3.9 \pm 2.3 h^{-1}$  Mpc,  $r_0^{\text{CIV}} = 7.5_{-1.4}^{+2.8} h^{-1}$  Mpc,  $r_0^{\text{LLS}} = 12.5_{-1.4}^{+2.7} h^{-1}$  Mpc, and  $r_0^{\text{SLLS}} = 14.0_{-2.7}^{+7.6} h^{-1}$  Mpc. It is astonishing (and possibly of concern) that the absorption systems known to trace the highest gas densities (DLAs) exhibit the smallest clustering amplitude. These amplitudes, which we emphasize are generally evaluated from clustering in the non-linear regime, suggest that the strongest H I absorption is less biased to the massive halos. Furthermore, our new measurements on C IV lend additional support to the conclusion of QPQ6 that optically thick gas with  $N_{\text{HI}} < 10^{20} \text{ cm}^{-2}$  is highly biased to the environment of massive halos. These results demand greater inspection within cosmological simulations, ideally incorporating a proper treatment of radiative transfer.

The excess of strong C IV absorbers around quasars implies that massive galaxies may contribute a significant fraction of the  $W_{1548} \geq 0.3\text{\AA}$  systems discovered along random quasar sightlines. Indeed, we estimated in § 5.3 that galaxies with  $M_{\text{halo}} \geq 10^{12} M_{\odot}$  can reproduce the observed incidence of strong Mg II absorbers. Integrating our cross-correlation function to  $R_{\perp} = 200$  kpc (and never allowing the covering fraction to exceed unity), we recover  $\ell(X)_{\text{CIV}} = 0.22$  or only  $\approx 10\%$  of the random incidence. Therefore, we find that if strong C IV occurs primarily within the CGM of galaxies than lower mass halos must dominate. This implies some tension with the clustering estimates described above, although the amplitude measured on large-scales (i.e. in the linear regime) corresponds to  $W_{1548} > 1\text{\AA}$ .

### 5.7. Do Quasars Quench Star Formation?

A principal focus of galaxy formation studies, possibly the primary focus, has been to identify and understand the physical process(es) that convert a blue, star-forming galaxy into a ‘red-and-dead’ system (e.g. Faber et al. 2007). In recent years, it has become fashionable to invoke feedback from AGN – thermal, radiative, mechanical – as the primary mechanism (e.g. Springel et al. 2005; Choi et al. 2014). Theorists have been motivated, at least in part, by the empirical revelation that all massive galaxies host super-massive black holes. One further recognizes that the astrophysics of gas accretion onto a supermassive black hole produces a tremendous output of energy that, if tapped, could easily influence the surrounding galaxy. A full study of AGN quenching in the context of QPQ may be the focus of a future manuscript; here, we offer a few comments and speculations.

Directly, we contend that the principal results of our QPQ experiment – the omnipresence of cool, enriched gas transverse to the sightline to quasars on scales to  $\approx 200$  kpc – *directly contradict the thesis that quasars quench star-formation*. On the contrary, this cool CGM represents a tremendous reservoir for current and future star-formation. Our conservative estimate gives  $M_{\text{CGM}}^{\text{cool}} > 10^{10} M_{\odot}$  of cool gas within these halos. At a temperature of  $T \approx 10^4$  K, this gas need cool no further to be accreted onto the central galaxy, and following Maller & Bullock (2004) we may estimate the infall time<sup>21</sup>. Those authors considered two processes: (i) ram pressure drag as the gas moves through a hot gas halo and (ii) cloud-cloud collisions (see also McDonald & Miralda-Escudé 1999). Their calculations for a low- $z$  halo with  $M_{\text{halo}} \approx 10^{12} M_{\odot}$  and  $M_{\text{CGM}}^{\text{cool}} = 2 \times 10^{10} M_{\odot}$  imply that cloud-cloud collisions dominate and that the infall time is approximately  $\tau_{\text{in}} \approx 1$  Gyr. For our higher mass and higher redshift halos, the infall times should be smaller. Therefore, we estimate a cool gas inflow rate of  $\dot{M}_{\text{CGM}}^{\text{cool}} \approx M_{\text{CGM}}^{\text{cool}}/\tau_{\text{in}} \approx 10 M_{\odot} \text{ yr}^{-1} (M_{\text{CGM}}^{\text{cool}}/10^{10} M_{\odot})(\tau_{\text{in}}/1 \text{ Gyr})^{-1}$ . Allowing for a considerably higher cool gas mass (probable) and/or a shorter infall time (also probable), we infer a mass inflow rate that likely exceeds  $100 M_{\odot} \text{ yr}^{-1}$ . This is comparable to the SFR estimated for galaxies hosting quasars (Rosario et al. 2013). We conclude that quasars are not quenching<sup>22</sup> star-formation at  $z \approx 2$  and that their halos contain a sufficient reservoir of cool gas to fuel the observed SFRs for at least 1 Gyr.

We may also offer a direct test to a recent prediction on AGN quenching from the literature. Choi et al. (2014) have implemented several forms of AGN feedback into a set of cosmological simulations studying the formation of early-type galaxies. Their analysis favors a scenario of radiative+mechanical feedback and they emphasize that thermal feedback over-predicts the observed X-ray luminosities of modern, early-type galaxies. From these models, they predicted the total gas surface density profiles  $\Sigma_{\text{gas}}(r)$  for the galaxies at  $z = 1.5$ , estimating

<sup>21</sup> The shortest timescale of interest is the dynamical, infall time of  $\sim 10^8$  yr.

<sup>22</sup> It is, however, without a doubt that quasars significantly affect the gas that they shine upon; this feedback, however, must be anisotropic.

$\Sigma_{\text{gas}} \approx 10^{5.5} M_{\odot} \text{ kpc}^{-2}$  at  $r \approx 100$  kpc (their Figure 7). This corresponds to  $N_{\text{H}} \approx 10^{19} \text{ cm}^{-2}$  assuming that helium contributes 25% of the mass. In QPQ3, we measured  $N_{\text{H}} = 10^{19.7} \text{ cm}^{-2}$  for an optically thick sightline at  $R_{\perp} = 108$  kpc and  $N_{\text{H}} = 10^{21} \text{ cm}^{-2}$  based on photoionization modeling. This exceeds the Choi et al. (2014) estimate by two orders-of-magnitude. In QPQ5, we argued that  $N_{\text{H}} > 10^{20} \text{ cm}^{-2}$  based on the very strong C II absorption. The results of this manuscript only strengthen the result. We conclude that the Choi et al. (2014) prescription removes too much gas from galactic halos and caution against similar AGN models for quenching star-formation.

## 6. SUMMARY AND CONCLUDING REMARKS

From a sample of 427 projected quasar pairs, we have analyzed the incidence and absorption strength of the C II 1334 and C IV 1548 transitions associated to the environment of the f/g quasar. These pairs have physical separations  $R_{\perp} \approx 39$  kpc to 1 Mpc at the f/g redshift  $z_{\text{fg}}$ , an average f/g quasar redshift of  $\langle z_{\text{fg}} \rangle = 2.41$ , and b/g quasar spectra with  $\text{S/N} \geq 9.5$  per  $\text{\AA}$  at the f/g H I Ly $\alpha$  transition. Measurements of the two-point correlation function of  $z \sim 2$  quasars imply they inhabit dark matter halos with mass  $M_{\text{halo}} = 10^{12.5} M_{\odot}$  and a characteristic virial radius of  $r_{\text{vir}} \approx 160$  kpc. Following our work on neutral hydrogen (QPQ6), we adopt an analysis window  $\delta v = \pm 1500 \text{ km s}^{-1}$  to account for uncertainties in  $z_{\text{fg}}$ .

We summarize our primary results and conclusions as:

- The galactic halos of luminous,  $z \sim 2$  quasars frequently exhibit strong C II 1334 absorption. For  $R_{\perp} \leq r_{\text{vir}}$ , we measure the covering fraction for  $W_{1334} \geq 0.2 \text{\AA}$  to be  $f_{\text{C}}^{1334} = 0.73 \pm 0.10$ . Beyond 200 kpc, the incidence rapidly declines and we measure  $f_{\text{C}}^{1334} = 0.08 \pm 0.03$ . We associate the observed C II 1334 absorption to the cool, CGM surrounding  $z \sim 2$  galaxies hosting quasars.
- The sightlines also frequently exhibit strong C IV 1548 absorption, with an excess incidence relative to random sightlines to at least 1 Mpc. We measure the cross-correlation between strong C IV 1548 absorption ( $W_{1548} \geq 0.3 \text{\AA}$ ) and quasars for  $R < 3h^{-1}$  comoving Mpc. Adopting a standard power-law description,  $\xi_{\text{CIV-Q}}(r) = (r/r_0)^{-\gamma}$ , a maximum likelihood analysis gives  $r_0 = 7.5_{-1.4}^{+2.8} h^{-1} \text{ Mpc}$  and  $\gamma = 1.7_{-0.2}^{+0.1}$ . These values are remarkably consistent with measurements from much larger (i.e. non-linear) scales (Vikas et al. 2013). This implies that the majority of C IV absorption may be associated to the massive halos ( $M > 10^{12} M_{\odot}$ ) of galaxies that cluster with the quasar host.
- Integrating column density estimates from the saturated C II 1334 profiles, we set a strict lower limit to the metal mass within  $r_{\text{vir}}$  of  $M_{\text{coolmetal}}^{\text{QPQ}} > 10^7 M_{\odot}$ . Adopting conservative saturation and ionization corrections, we conservatively estimate  $M_{\text{coolmetal}}^{\text{QPQ}} > 10^8 M_{\odot}$ . These values exceed estimates for the metal-mass of the cool CGM around present-day  $L^*$  galaxies (Werk et al. 2014). These

metals likely represent the early enrichment of halo gas predicted by chemical evolution models that study the formation and enrichment of the intra-group and intracluster medium.

- We study the integrated incidence of strong, low-ion absorption arising from massive,  $z \sim 2$  halos. Under the assumption that all halos with mass  $M_{\text{halo}} > 10^{12} M_{\odot}$  exhibit properties similar to the QPQ sample and that strong C II absorption indicates strong Mg II absorption (as observed), we estimate the incidence of strong Mg II lines to be  $\ell(X)_{\text{MgII}}^{\text{QPQ}}(> 1\text{\AA}) = 0.11$  for gas within 200 kpc of these massive halos. This integrated incidence is consistent with surveys of strong Mg II along random sightlines (Seyffert et al. 2013), implying that the majority of such absorbers are physically associated to massive halos.
- We compare the incidence and absorption strength of low-ions (C II, Mg II) between the QPQ-CGM and that for LBGs at  $z \sim 2$ , quasar hosts at  $z \sim 1$ , LRGs at  $z \sim 0.5$  and  $L^*$  and sub- $L^*$  galaxies at  $z \sim 0$ . On a physical scale,  $R_{\perp} < 200$  kpc, we conclude that the massive  $z \sim 2$  halos hosting quasars represents the pinnacle of the cool CGM. This conclusion is supported by our previous analysis of H I Ly $\alpha$  absorption (QPQ6).
- We examine the characteristics of the cool CGM for galaxies ranging from  $z \sim 0$  dwarfs to massive,  $z \sim 0.5$  LRGs, and the halos hosting quasars at  $z \sim 1$  and  $z \sim 2$ . We argue that the cool CGM is not dominated by astrophysical processes related to active star-formation or AGN feedback, nor cold gas accretion. Instead, we propose that the cool CGM properties track halo mass with more massive halos exhibiting a more substantial cool CGM. Of course, SFR and gas accretion are expected to scale with halo mass but we assert that the cool CGM primarily tracks the cumulative growth of galactic halos and their integrated enrichment history.

The results presented in this manuscript and previous publications of our QPQ survey have defined the incidence and absorption strength of cool gas surrounding the massive galaxies hosting luminous  $z \sim 2$  quasars. To our surprise, these galaxies exhibit a cool CGM with properties exceeding any previous set of galaxies, including those generated within cosmological simulations. These results, therefore, inspire the following lines of future inquiry:

1. A study of the CGM at high spectral resolution to resolve properties of the gas: H I surface density, kinematics, ionization state, metallicity, etc. The majority of data analysis to date has been on low-resolution spectra with limited diagnostic power. A manuscript presenting 11 sightlines with data similar to QPQ3 is forthcoming (Lau et al. in prep.).
2. A survey of the CGM surrounding halos with comparable mass to the hosts of  $z \sim 2$  quasars ( $\sim 10^{12.5} M_{\odot}$ ) but without a luminous AGN. This would provide a test of our working hypothesis that

the presence of a luminous quasar has minimal effect on the gas at CGM scales (hundreds kpc). One viable approach is to survey the CGM of sub-mm galaxies, whose two-point clustering measurements are comparable to luminous quasars (White et al. 2012). Ongoing efforts to identify such sources across a wide area of the sky may yield several tens of projected SMG-quasar pairs for study.

3. Study the CGM and surrounding IGM with narrow-band and IFU imaging (Cantalupo et al. 2014; Martin et al. 2014).
4. New theoretical studies on the complex astrophysics of the CGM at  $z > 2$ . It is now evident that even state-of-the-art zoom-in simulations have insufficient resolution to properly capture the astrophysics of this cool gas (e.g., QPQ6 Crighton et al. 2014; Fumagalli et al. 2014). Researchers may need to input sub-grid models, akin to those for star-formation and associated feedback, to examine global trends and establish the implications for galaxy formation.

JXP dedicates this manuscript to the memory of Arthur M. Wolfe, who inspired his careers in the field. JXP would also like to thank the Aspen Institute for Physics where discussions at the Winter Conference stimulated several aspects of this work. JXP and ML acknowledge support from the National Science Foundation (NSF) grant AST-1010004 and AST-1412981. JXP thanks the Alexander von Humboldt foundation for a visitor fellowship to the MPIA where part of this work was performed, as well as the staff at MPIA for their hospitality during his visits. JFH acknowledges generous support from the Alexander von Humboldt foundation in the context of the Sofja Kovalevskaja Award. The Humboldt foundation is funded by the German Federal Ministry for Education and Research. We thank D. Bowen for providing the  $f_C$  values presented in the Appendix and R. Bordoloi for providing measurements from the COS-Dwarfs survey in advance of publication. We further acknowledge R. Yates for providing outputs from his chemical evolution models in advance of publication. We acknowledge the contributions of Sara Ellison, George Djorgovski, Crystal Martin, Rob Simcoe, and Kate Rubin in obtaining some of the spectra analyzed in this manuscript.

Much of the data presented herein were obtained at the W.M. Keck Observatory, which is operated as a scientific partnership among the California Institute of Technology, the University of California, and the National Aeronautics and Space Administration. The Observatory was made possible by the generous financial support of the W.M. Keck Foundation. Some of the Keck data were obtained through the NSF Telescope System Instrumentation Program (TSIP), supported by AURA through the NSF under AURA Cooperative Agreement AST 01-32798 as amended.

Some of the data herein were obtained at the Gemini Observatory, which is operated by the Association of Universities for Research in Astronomy, Inc., under a cooperative agreement with the NSF on behalf of the Gemini

partnership: the NSF (United States), the Science and Technology Facilities Council (United Kingdom), the National Research Council (Canada), CONICYT (Chile), the Australian Research Council (Australia), Ministério da Ciência, Tecnologia e Inovação (Brazil) and Ministerio de Ciencia, Tecnología e Innovación Productiva (Argentina).

gentina).

The authors wish to recognize and acknowledge the very significant cultural role and reverence that the summit of Mauna Kea has always had within the indigenous Hawaiian community. We are most fortunate to have the opportunity to conduct observations from this mountain.

#### REFERENCES

- Abazajian, K. N., et al. 2009, *ApJS*, 182, 543  
 Adelberger, K. L., Shapley, A. E., Steidel, C. C., Pettini, M., Erb, D. K., & Reddy, N. A. 2005a, *ApJ*, 629, 636  
 Adelberger, K. L., Steidel, C. C., Pettini, M., Shapley, A. E., Reddy, N. A., & Erb, D. K. 2005b, *ApJ*, 619, 697  
 Adelberger, K. L., Steidel, C. C., Shapley, A. E., & Pettini, M. 2003, *ApJ*, 584, 45  
 Ahn, C. P., et al. 2012, *ApJS*, 203, 21  
 Akerman, C. J., Carigi, L., Nissen, P. E., Pettini, M., & Asplund, M. 2004, *A&A*, 414, 931  
 Anderson, M. E., Bregman, J. N., & Dai, X. 2013, *ApJ*, 762, 106  
 Andreon, S. 2012, *A&A*, 546, A6  
 Andrews, H., et al. 2013, *ApJ*, 774, 40  
 Antonucci, R. 1993, *ARA&A*, 31, 473  
 Arrigoni, M., Trager, S. C., & Somerville, R. S. 2010, *ArXiv e-prints*  
 Arrigoni-Battaia, F., Hennawi, J. F., & Prochaska, J. X. 2014, *MNRAS*, submitted  
 Bahcall, J. N., & Peebles, P. J. E. 1969, *ApJ*, 156, L7+  
 Bahcall, J. N., & Spitzer, L. J. 1969, *ApJ*, 156, L63  
 Bajtlik, S., Duncan, R. C., & Ostriker, J. P. 1988, *ApJ*, 327, 570  
 Baldi, A., Ettori, S., Molendi, S., Balestra, I., Gastaldello, F., & Tozzi, P. 2012, *A&A*, 537, A142  
 Becker, G. D., Hewett, P. C., Worseck, G., & Prochaska, J. X. 2013, *MNRAS*, 430, 2067  
 Bergeron, J. 1986, *A&A*, 155, L8  
 Bielby, R., et al. 2013, *MNRAS*, 430, 425  
 Boksenberg, A., Sargent, W. L. W., & Rauch, M. 2003, *ArXiv Astrophysics e-prints*  
 Bonaparte, I., Matteucci, F., Recchi, S., Spitoni, E., Pipino, A., & Grieco, V. 2013, *MNRAS*, 435, 2460  
 Bordoloi, R., et al. 2014, *ArXiv e-prints*  
 Borthakur, S., Heckman, T., Strickland, D., Wild, V., & Schiminovich, D. 2013, *ApJ*, 768, 18  
 Bouché, N., et al. 2012, *MNRAS*, 419, 2  
 Bovy, J., et al. 2011, *ApJ*, 729, 141  
 —. 2012, *ApJ*, 749, 41  
 Bowen, D. V., & Chelouche, D. 2011, *ApJ*, 727, 47  
 Bowen, D. V., et al. 2006, *ApJ*, 645, L105  
 Cantalupo, S., Arrigoni-Battaia, F., Prochaska, J. X., Hennawi, J. F., & Madau, P. 2014, *Nature*, 506, 63  
 Chelouche, D., Ménard, B., Bowen, D. V., & Gnat, O. 2008, *ApJ*, 683, 55  
 Chen, H., Helsby, J. E., Gauthier, J., Shectman, S. A., Thompson, I. B., & Tinker, J. L. 2010a, *ApJ*, 714, 1521  
 Chen, H.-W. 2012, *MNRAS*, 427, 1238  
 Chen, H.-W., Lanzetta, K. M., & Webb, J. K. 2001, *ApJ*, 556, 158  
 Chen, H.-W., Wild, V., Tinker, J. L., Gauthier, J.-R., Helsby, J. E., Shectman, S. A., & Thompson, I. B. 2010b, *ApJ*, 724, L176  
 Choi, E., Ostriker, J. P., Naab, T., Oser, L., & Moster, B. P. 2014, *ArXiv e-prints*  
 Churchill, C. W., Trujillo-Gomez, S., Nielsen, N. M., & Kacprzak, G. G. 2013, *ArXiv e-prints*  
 Conroy, C., Shapley, A. E., Tinker, J. L., Santos, M. R., & Lemson, G. 2008, *ApJ*, 679, 1192  
 Cooke, J., Wolfe, A. M., Gawiser, E., & Prochaska, J. X. 2006, *ApJ*, 636, L9  
 Cooksey, K. L., Kao, M. M., Simcoe, R. A., O’Meara, J. M., & Prochaska, J. X. 2013, *ApJ*, 763, 37  
 Coppin, K. E. K., et al. 2008, *MNRAS*, 389, 45  
 Creasey, P., Theuns, T., & Bower, R. G. 2013, *MNRAS*, 429, 1922  
 Crighton, N. H. M., et al. 2011, *MNRAS*, 414, 28  
 Crighton, N. H. M., Hennawi, J. F., & Prochaska, J. X. 2013, *ApJ*, 776, L18  
 Crighton, N. H. M., Hennawi, J. F., Simcoe, R. A., Cooksey, K. L., Murphy, M. T., Fumagalli, M., Prochaska, J. X., & Shanks, T. 2014, *ArXiv e-prints*  
 Croft, R. A. C. 2004, *ApJ*, 610, 642  
 Crotts, A. P. S. 1989, *ApJ*, 336, 550  
 Davis, M., & Peebles, P. J. E. 1977, *ApJS*, 34, 425  
 Diemand, J., Kuhlen, M., & Madau, P. 2007, *ApJ*, 667, 859  
 Diemer, B., More, S., & Kravtsov, A. V. 2013, *ApJ*, 766, 25  
 D’Odorico, V., Calura, F., Cristiani, S., & Viel, M. 2010, *MNRAS*, 401, 2715  
 Dunlop, J. S., McLure, R. J., Kukula, M. J., Baum, S. A., O’Dea, C. P., & Hughes, D. H. 2003, *MNRAS*, 340, 1095  
 Ebeling, H., Stephenson, L. N., & Edge, A. C. 2014, *ApJ*, 781, L40  
 Faber, S. M., et al. 2007, *ApJ*, 665, 265  
 Fanidakis, N., Macciò, A. V., Baugh, C. M., Lacey, C. G., & Frenk, C. S. 2013, *MNRAS*, 436, 315  
 Farina, E. P., Falomo, R., Decarli, R., Treves, A., & Kotilainen, J. K. 2013, *MNRAS*, 429, 1267  
 Farina, E. P., Falomo, R., Scarpa, R., Decarli, R., Treves, A., & Kotilainen, J. K. 2014, *ArXiv e-prints*  
 Ferland, G. J., et al. 2013, *RMXAA*, 49, 137  
 Font-Ribera, A., et al. 2013, *JCAP*, 5, 18  
 Fumagalli, M., Hennawi, J. F., Prochaska, J. X., Kasen, D., Dekel, A., Ceverino, D., & Primack, J. 2014, *ApJ*, 780, 74  
 Fumagalli, M., O’Meara, J. M., & Prochaska, J. X. 2011a, *Science*, 334, 1245  
 Fumagalli, M., O’Meara, J. M., Prochaska, J. X., & Worseck, G. 2013, *ApJ*, 775, 78  
 Fumagalli, M., Prochaska, J. X., Kasen, D., Dekel, A., Ceverino, D., & Primack, J. R. 2011b, *MNRAS*, 418, 1796  
 Gauthier, J.-R., & Chen, H.-W. 2011, *MNRAS*, 418, 2730  
 Haardt, F., & Madau, P. 2012, *ApJ*, 746, 125  
 Hennawi, J. F. 2004, Ph.D. Thesis  
 Hennawi, J. F., et al. 2010, *ApJ*, 719, 1672  
 Hennawi, J. F., & Prochaska, J. X. 2007, *ApJ*, 655, 735  
 —. 2013, *ApJ*, 766, 58 (QPQ4)  
 Hennawi, J. F., et al. 2006a, *ApJ*, 651, 61  
 —. 2006b, *AJ*, 131, 1  
 Hopkins, P. F., Richards, G. T., & Hernquist, L. 2007, *ApJ*, 654, 731  
 Ivezić, Ž., et al. 2002, *AJ*, 124, 2364  
 Jenkins, E. B. 2009, *ApJ*, 700, 1299  
 Kwak, K., Henley, D. B., & Shelton, R. L. 2011, *ApJ*, 739, 30  
 Lanzetta, K. M. 1993, in *ASSL Vol. 188: The Environment and Evolution of Galaxies*, ed. J. M. Shull & H. A. Thronson, 237–4  
 Lee, K.-G., et al. 2013, *AJ*, 145, 69  
 Lee, K.-G., Suzuki, N., & Spergel, D. N. 2012, *AJ*, 143, 51  
 Loewenstein, M. 2013, *ApJ*, 773, 52  
 Lopez, S., et al. 2008, *ApJ*, 679, 1144  
 Madau, P., Ferrara, A., & Rees, M. J. 2001, *ApJ*, 555, 92  
 Mainieri, V., et al. 2011, *A&A*, 535, A80  
 Maller, A. H., & Bullock, J. S. 2004, *MNRAS*, 355, 694  
 Mandelbaum, R., Tasitsiomi, A., Seljak, U., Kravtsov, A. V., & Wechsler, R. H. 2005, *MNRAS*, 362, 1451  
 Martin, A. M., Papastergis, E., Giovanelli, R., Haynes, M. P., Springob, C. M., & Stierwalt, S. 2010a, *ApJ*, 723, 1359  
 Martin, C. L. 2005, *ApJ*, 621, 227  
 Martin, C. L., Scannapieco, E., Ellison, S. L., Hennawi, J. F., Djorgovski, S. G., & Fournier, A. P. 2010b, *ApJ*, 721, 174  
 Martin, D. C., Chang, D., Matuszewski, M., Morrissey, P., Rahman, S., Moore, A., & Steidel, C. C. 2014, *ApJ*, 786, 106  
 Matejek, M. S., & Simcoe, R. A. 2012, *ApJ*, 761, 112  
 Matsuda, Y., et al. 2004, *AJ*, 128, 569  
 Matteucci, F., & Gibson, B. K. 1995, *A&A*, 304, 11  
 McDonald, P., & Miralda-Escudé, J. 1999, *ApJ*, 519, 486

- Ménard, B., Wild, V., Nestor, D., Quider, A., Zibetti, S., Rao, S., & Turnshek, D. 2011, *MNRAS*, 417, 801
- Mitchell, R. J., Culhane, J. L., Davison, P. J. N., & Ives, J. C. 1976, *MNRAS*, 175, 29P
- Mo, H. J., & White, S. D. M. 1996, *MNRAS*, 282, 347
- Moller, P., & Kjaergaard, P. 1992, *A&A*, 258, 234
- Moster, B. P., Somerville, R. S., Maulbetsch, C., van den Bosch, F. C., Macciò, A. V., Naab, T., & Oser, L. 2010, *ApJ*, 710, 903
- Narayanan, A., Charlton, J. C., Misawa, T., Green, R. E., & Kim, T.-S. 2008, *ApJ*, 689, 782
- Nestor, D. B., Turnshek, D. A., & Rao, S. M. 2005, *ApJ*, 628, 637
- Nielsen, N. M., Churchill, C. W., Kacprzak, G. G., & Murphy, M. T. 2013, *ApJ*, 776, 114
- O’Meara, J. M., Prochaska, J. X., Chen, H.-W., & Madau, P. 2011, *ApJS*, 195, 16
- Oppenheimer, B. D., & Davé, R. 2006, *MNRAS*, 373, 1265
- Ostriker, J. P., & Heisler, J. 1984, *ApJ*, 278, 1
- Peebles, M. S., Werk, J. K., Tumlinson, J., Oppenheimer, B. D., Prochaska, J. X., Katz, N., & Weinberg, D. H. 2013, *ArXiv e-prints*
- Pettini, M., Kellogg, M., Steidel, C. C., Dickinson, M., Adelberger, K. L., & Giavalisco, M. 1998, *ApJ*, 508, 539
- Portinari, L., Moretti, A., Chiosi, C., & Sommer-Larsen, J. 2004, *ApJ*, 604, 579
- Prochaska, J. X., & Hennawi, J. F. 2009, *ApJ*, 690, 1558
- Prochaska, J. X., et al. 2013a, *ApJ*, 776, 136
- Prochaska, J. X., Hennawi, J. F., & Simcoe, R. A. 2013b, *ApJ*, 762, L19 (QPQ5)
- Prochaska, J. X., Weiner, B., Chen, H.-W., Mulchaey, J., & Cooksey, K. 2011, *ApJ*, 740, 91
- Prochaska, J. X., & Wolfe, A. M. 2009, *ApJ*, 696, 1543
- Prochter, G. E., Prochaska, J. X., & Burles, S. M. 2006, *ApJ*, 639, 766
- Quashnock, J. M., & vanden Berk, D. E. 1998, *ApJ*, 500, 28
- Rakic, O., Schaye, J., Steidel, C. C., Booth, C. M., Dalla Vecchia, C., & Rudie, G. C. 2013, *MNRAS*, 433, 3103
- Rakic, O., Schaye, J., Steidel, C. C., & Rudie, G. C. 2012, *ApJ*, 751, 94
- Rao, S. M., Turnshek, D. A., & Nestor, D. B. 2006, *ApJ*, 636, 610
- Renzini, A., Ciotti, L., D’Ercole, A., & Pellegrini, S. 1993, *ApJ*, 419, 52
- Ribaudo, J., Lehner, N., & Howk, J. C. 2011, *ApJ*, 736, 42
- Richardson, J., Zheng, Z., Chatterjee, S., Nagai, D., & Shen, Y. 2012, *ApJ*, 755, 30
- Rosario, D. J., et al. 2013, *A&A*, 560, A72
- Rubin, K. H. R., Prochaska, J. X., Koo, D. C., Phillips, A. C., Martin, C. L., & Winstrom, L. O. 2013, *ArXiv e-prints*
- Rudie, G. C., Steidel, C. C., Shapley, A. E., & Pettini, M. 2013, *ApJ*, 769, 146
- Rudie, G. C., et al. 2012, *ApJ*, 750, 67
- Sasaki, T., Matsushita, K., & Sato, K. 2014, *ApJ*, 781, 36
- Scherrer, R. J., & Weinberg, D. H. 1998, *ApJ*, 504, 607
- Scott, J., Bechtold, J., Dobrzycki, A., & Kulkarni, V. P. 2000, *ApJS*, 130, 67
- Seyffert, E. N., Cooksey, K. L., Simcoe, R. A., O’Meara, J. M., Kao, M. M., & Prochaska, J. X. 2013, *ApJ*, 779, 161
- Shen, S., Madau, P., Aguirre, A., Guedes, J., Mayer, L., & Wadsley, J. 2011, *ArXiv e-prints*
- Shen, S., Madau, P., Conroy, C., Governato, F., & Mayer, L. 2013a, *ArXiv e-prints*
- Shen, S., Madau, P., Guedes, J., Mayer, L., Prochaska, J. X., & Wadsley, J. 2013b, *ApJ*, 765, 89
- Shen, Y., et al. 2013c, *ApJ*, 778, 98
- . 2007, *AJ*, 133, 2222
- Sijacki, D., Springel, V., di Matteo, T., & Hernquist, L. 2007, *MNRAS*, 380, 877
- Silk, J., & Rees, M. J. 1998, *A&A*, 331, L1
- Simcoe, R. A., Sargent, W. L. W., Rauch, M., & Becker, G. 2006, *ApJ*, 637, 648
- Simpson, J. M., et al. 2012, *MNRAS*, 426, 3201
- Sivanandam, S., Zabludoff, A. I., Zaritsky, D., Gonzalez, A. H., & Kelson, D. D. 2009, *ApJ*, 691, 1787
- Spitzer, L. 1978, *Physical processes in the interstellar medium* (New York Wiley-Interscience, 1978. 333 p.)
- Springel, V., Di Matteo, T., & Hernquist, L. 2005, *ApJ*, 620, L79
- Steidel, C. C. 1993, in *ASSL Vol. 188: The Environment and Evolution of Galaxies*, ed. J. M. Shull & H. A. Thronson, 263–+
- Steidel, C. C., Erb, D. K., Shapley, A. E., Pettini, M., Reddy, N., Bogosavljević, M., Rudie, G. C., & Rakic, O. 2010, *ApJ*, 717, 289
- Stinson, G. S., et al. 2012, *MNRAS*, 425, 1270
- Stocke, J. T., Keeney, B. A., Danforth, C. W., Shull, J. M., Froning, C. S., Green, J. C., Penton, S. V., & Savage, B. D. 2013, *ApJ*, 763, 148
- Tejos, N., et al. 2014, *MNRAS*, 437, 2017
- Thom, C., et al. 2012, *ApJ*, 758, L41
- Tumlinson, J., et al. 2013, *ApJ*, 777, 59
- . 2011, *Science*, 334, 948
- Turner, M. L., Schaye, J., Steidel, C. C., Rudie, G. C., & Strom, A. L. 2014, *ArXiv e-prints*
- van de Voort, F., & Schaye, J. 2012, *MNRAS*, 423, 2991
- Veilleux, S., et al. 2009, *ApJ*, 701, 587
- . 2013, *ApJ*, 776, 27
- Vikas, S., et al. 2013, *ApJ*, 768, 38
- Wang, R., et al. 2008, *ApJ*, 687, 848
- Weiner, B. J., et al. 2009, *ApJ*, 692, 187
- Werk, J. K., Prochaska, J. X., Thom, C., Tumlinson, J., Tripp, T. M., O’Meara, J. M., & Peebles, M. S. 2013, *ApJS*, 204, 17
- Werk, J. K., et al. 2014, *ArXiv e-prints*
- Whitaker, K. E., van Dokkum, P. G., Brammer, G., & Franx, M. 2012, *ApJ*, 754, L29
- White, M., et al. 2012, *MNRAS*, 424, 937
- Wild, V., et al. 2008, *MNRAS*, 388, 227
- Yates, R. 2014, *MNRAS*, submitted
- Yoon, J. H., & Putman, M. E. 2013, *ApJ*, 772, L29
- Zaritsky, D., Gonzalez, A. H., & Zabludoff, A. I. 2004, *ApJ*, 613, L93
- Zhu, G., et al. 2014, *MNRAS*
- Zwaan, M. A., Meyer, M. J., Staveley-Smith, L., & Webster, R. L. 2005a, *MNRAS*, 359, L30
- Zwaan, M. A., van der Hulst, J. M., Briggs, F. H., Verheijen, M. A. W., & Ryan-Weber, E. V. 2005b, *MNRAS*, 364, 1467

## APPENDIX

**APPENDIX A: C IV Search**

To enable the evaluation of the cross-correlation of strong C IV absorption to quasars  $\xi_{\text{CIV-Q}}$  from our dataset (§ 5.6), we have first performed a survey for strong C IV absorption ( $W_{1548} \geq 0.3\text{\AA}$ ) along random samples of quasar sightlines. Although previous surveys for C IV absorption have been performed (e.g. Boksenberg et al. 2003; D’Odorico et al. 2010; Cooksey et al. 2013), none of these were fully satisfactory for our planned analysis. Therefore, we chose to survey a modest sample ( $\sim 80$ ) of quasar spectra taken from the SDSS survey. Although we have access to spectra with much higher resolution, these SDSS spectra have comparable data quality to the majority of our quasar pair sample and therefore suffers from similar systematic uncertainties. Specifically, we analyzed the SDSS spectra of 78 quasars drawn randomly from the cohort defined by O’Meara et al. (2011) to survey  $z < 2$  Lyman limit absorption using UV spectrometers on the Hubble Space Telescope (*HST*). These have magnitudes  $g < 18.3$ , yielding relatively high quality SDSS data, and emission redshifts  $z_{\text{em}} \approx 2.5$ . From these, we excluded any quasar exhibiting very strong associated absorption at  $z \approx z_{\text{em}}$ .

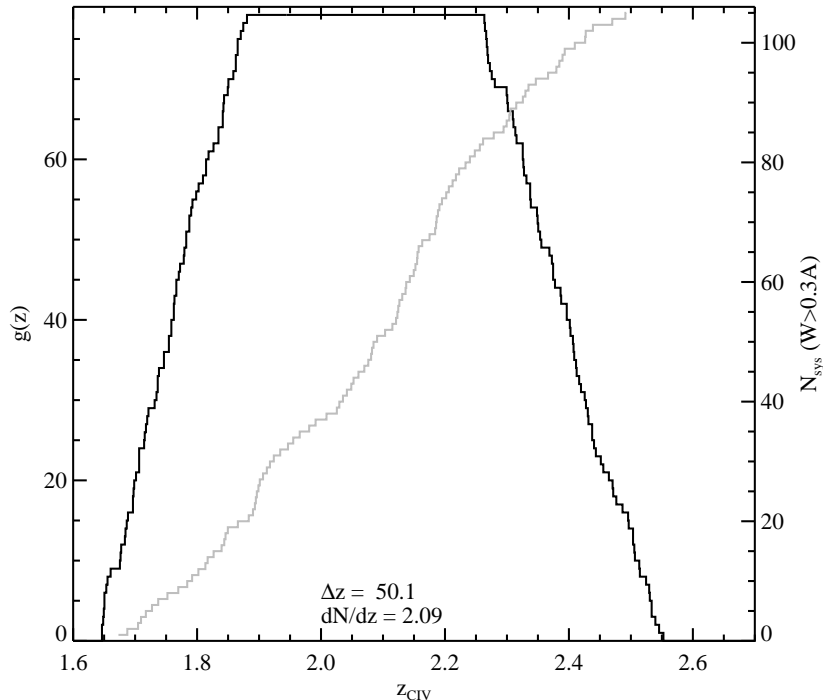


FIG. 17.— The black curve depicts the sensitivity function  $g(z)$  of the survey we have performed for strong C IV 1548 absorption ( $W_{1548} \geq 0.3\text{\AA}$ ) in a set of SDSS quasar spectra defined by O’Meara et al. (2011). The total search path  $\Delta z = \int g(z)dz = 50.1$ . The gray curve shows the cumulative incidence of intervening C IV systems satisfying the  $W_{1548}$  limit discovered in the survey. This gives an estimate for the incidence of  $\ell(z) = 2.09$  with an approximately 10% Poisson error. Previous estimations are in good agreement with our more precise measurement (e.g. Boksenberg et al. 2003; D’Odorico et al. 2010; Cooksey et al. 2013).

A majority of these data had been previously surveyed for C IV absorption by Cooksey et al. (2013). We began our search with their C IV candidate list<sup>23</sup>, vetted these candidates and identified new systems by-eye using custom software. We adopted and then modified, as necessary, the quasar continua implemented by those authors using a similar algorithm as for the quasar pair analysis. Table 5 lists the quasars surveyed and all of the C IV absorption systems discovered. We measured equivalent widths  $W_{1548}$  for these systems using the same algorithms for the quasar pair spectra (§ 3).

Figure 17 presents a summary of the survey path and the set of C IV absorbers discovered. For completeness, we have listed all of the systems, not only those that enter into the statistical sample. Note that for our equivalent width limit of  $0.3\text{\AA}$ , such systems represent  $> 5\sigma$  detections. Regarding the statistical survey, we limit the search of each quasar to the wavelengths  $\lambda_r \geq 1238.8\text{\AA}$  in the quasar rest-frame and to the spectral region  $\delta v \leq -4000\text{km s}^{-1}$  of the emission redshift. These criteria define the  $z_{\text{start}}$  and  $z_{\text{end}}$  values listed in Table 5. For the 78 quasars surveyed, we constructed a total redshift path  $\Delta z = 50.1$  and have discovered 105 systems satisfying  $W_{1548} > 0.3\text{\AA}$  within the search regions. This gives an incidence of strong C IV 1548 absorption at  $\langle z \rangle = 2.1$  of  $\ell_{0.3\text{\AA}}^{\text{CIV}}(z) = 2.1 \pm 0.2$ . The error reported reflects Poisson uncertainty from limited sample size. We estimate an additional  $\approx 10\%$  systematic uncertainty owing to continuum placement, line-blending, and mis-identifications (e.g. a pair of coincident absorption lines masquerading as a C IV doublet).

We may compare our results to previous estimates of  $\ell^{\text{CIV}}(z)$  for strong C IV systems. Cooksey et al. (2013) reported  $\ell_{0.6\text{\AA}}^{\text{CIV}}(z) = 1.04$  for  $W_{1548} \geq 0.6\text{\AA}$ . For  $W_{1548} \geq 0.3\text{\AA}$ , they estimate a completeness of less than 50% but correct for this incompleteness to estimate  $\ell_{0.3\text{\AA}}^{\text{CIV}}(z) = 2.3$ . This value is fully consistent with our results given the uncertainties associated with incompleteness and sample variance. D’Odorico et al. (2010) performed a C IV survey in high quality, echelle spectra at  $z \sim 2$  achieving a sensitivity to  $W_{1548} \ll 0.3\text{\AA}$ . They discovered 28 C IV absorbers with  $W_{1548} > 0.3\text{\AA}$  within their  $\Delta z = 17.9$  survey path giving  $\ell_{0.3\text{\AA}}^{\text{CIV}}(z) = 1.6$ , but they defined systems within windows of only  $50\text{ km s}^{-1}$  which is below the SDSS resolution and much lower than our analysis windows. We consider their results to be fully consistent, especially given their large sample variance.

## APPENDIX B: Luminous Red Galaxy Analysis

To generate the CGM maps of Mg II for the LRG sample (Figure 11), we made the following assumptions and approximations. First, we adopted the covering fractions  $f_C$  measured by Bowen & Chelouche (2011) for strong Mg II absorbers ( $W_{2796} > 0.3\text{\AA}$ ). Specifically, they measured  $f_C = [0.245, 0.193, 0.032, 0.01]$  for  $R_{\perp} = [25., 75., 125., 175]\text{kpc}$ . Although these results were derived from a photometrically-selected sample of LRGs, they are in good agreement with

<sup>23</sup> <http://ucolick.org/~xavier/SDSSCIV/index.html>

TABLE 5  
SDSS C IV SURVEY

Quasar	$z_q$	$z_{\text{start}}^a$	$z_{\text{end}}^b$	$z_{\text{CIV}}$ (Å)	$W_{\text{CIV}}$ (Å)	$\sigma(W_{\text{CIV}})$
J023924.48–090138.6	2.472	1.778	2.426	2.393	0.44	0.04
			2.495	1.17	0.03	
J075158.65+424522.9	2.453	1.763	2.407	2.137	0.53	0.03
			2.305	0.65	0.03	
J075547.83+220450.1	2.319	1.656	2.275	1.794	0.44	0.06
			2.284	0.17	0.04	
J080132.02+192317.5	2.542	1.834	2.495	2.117	0.24	0.04
J080620.47+504124.4	2.432	1.746	2.387	1.794	0.08	0.04
			1.810	0.70	0.04	
J081014.62+204021.4	2.484	1.788	2.438	1.780	0.73	0.03
			1.817	0.34	0.03	
			2.084	0.42	0.03	
			2.190	0.45	0.03	
			2.361	0.19	0.03	
J081114.66+172057.4	2.307	1.646	2.263			
J083326.82+081552.0	2.572	1.858	2.525	2.071	0.19	0.05
			2.187	1.14	0.04	
J085417.60+532735.2	2.418	1.735	2.373			
J091301.01+422344.7	2.311	1.649	2.267	1.711	0.41	0.04
			1.897	1.62	0.05	
			2.046	0.43	0.04	
			2.068	0.37	0.04	
			2.207	1.01	0.05	
			2.316	0.24	0.03	

NOTE. — [The complete version of this table is in the electronic edition of the Journal. The printed edition contains only a sample.]

<sup>a</sup> Starting redshift for the C IV search. Defined as  $(1 + z_q) * 1238.8/1548.195 - 1$  with  $z_q$  the emission redshift of the quasar.

<sup>b</sup> Ending redshift for the C IV search. This is defined as  $4000 \text{ km s}^{-1}$  blueward of the quasar redshift.

the (smaller) spectroscopic study of Gauthier & Chen (2011).

Second, we assume that the absorbers associated with LRGs and having  $W_{2796} > 0.3\text{Å}$  exhibit a  $W_{2796}$  distribution similar to the intervening population along ‘random’ quasar sightlines. This  $W_{2796}$  distribution is well-described by an exponential,  $f(W_{2796}) \propto \exp[-W_{2796}/W_{2796}^*]$ , with  $W_{2796}^* = 0.7\text{Å}$  (Nestor et al. 2005; Prochter et al. 2006). Integrating this distribution from  $0.3\text{Å}$  to  $\infty$ , we calculate an average equivalent width  $\langle W_{2796} \rangle^S = 1\text{Å}$  for these strong systems. This means that an ensemble of sightlines with a covering fraction  $f_C^S$  to strong Mg II absorption has an average equivalent width  $f_C^S \langle W_{2796} \rangle^S$ . We further assume that sightlines with  $W_{2796} < 0.3\text{Å}$  have an equivalent width distribution that follows a power-law to  $0.01\text{Å}$  with exponent  $\gamma = -3$ . This gives an average equivalent width for such weak absorbers,  $\langle W_{2796} \rangle^W = 0.02\text{Å}$ . Altogether, an ensemble of sightlines has

$$\langle W_{2796} \rangle = (1 - f_C^S) \langle W_{2796} \rangle^W + f_C^S \langle W_{2796} \rangle^S \quad (1)$$

Finally, to generate the CGM maps for LRGs in Figure 11, we combine the  $f_C$  values of Bowen & Chelouche (2011) and the  $W_{2796}$  distributions for weak/strong systems. Together these provide the  $W_{2796}$  distribution shown in Figure 11 as a function of  $R_\perp$ .

Figure 18 presents the  $f_C$  values from the literature for a limiting equivalent width of  $0.3\text{Å}$  versus impact parameter (Bowen & Chelouche 2011; Gauthier & Chen 2011). Overplotted on these data is the curve showing the  $f_C$  values required to reproduce the measured  $\langle W_{2796} \rangle$  values from Z14, ignoring the contribution from weak absorbers (i.e. the first term in Equation 1). At  $R_\perp < 100 \text{ kpc}$  it is evident that a large  $f_C$  value is required to reproduce the observations. We conclude that the central, red-and-dead galaxy of these massive halos exhibits a cool and enriched CGM.

At larger radii ( $R_\perp \approx r_{\text{vir}}$ ), however, the measurements may be reproduced with a very small cover fraction ( $f_C < 5\%$ ), consistent with the low  $f_C$  values inferred from direct analysis. We contend that the  $\langle W_{2796} \rangle$  measurements of Z14 are dominated by such rare sightlines. We further posit that these represent sightlines penetrating the gas associated to satellite galaxies of the dark matter halos hosting LRGs. Such gas may be the ISM of these galaxies and/or their own ‘local’ CGM. One need not invoke an extremely diffuse medium with  $W_{2796} \ll 0.3\text{Å}$  throughout the LRG halo to explain the Z14 measurements. And, we also emphasize that this interpretation follows from the results on Mg II observed for the CGM of lower mass populations (e.g. Werk et al. 2013).

Taking the above conclusion one step further, we may test whether all of the mass in the Z14 measurements at  $R_\perp > r_{\text{vir}}$  could be associated to the ISM of individual galaxies. Integrating the mass profile of their 2-halo term, they represent an average ratio of  $\text{Mg}^+$  ions to dark matter:  $\rho(\text{Mg}^+)/\rho_{\text{DM}} \approx 10^{-8}$ . Now consider the mass density of  $\text{Mg}^+$  in

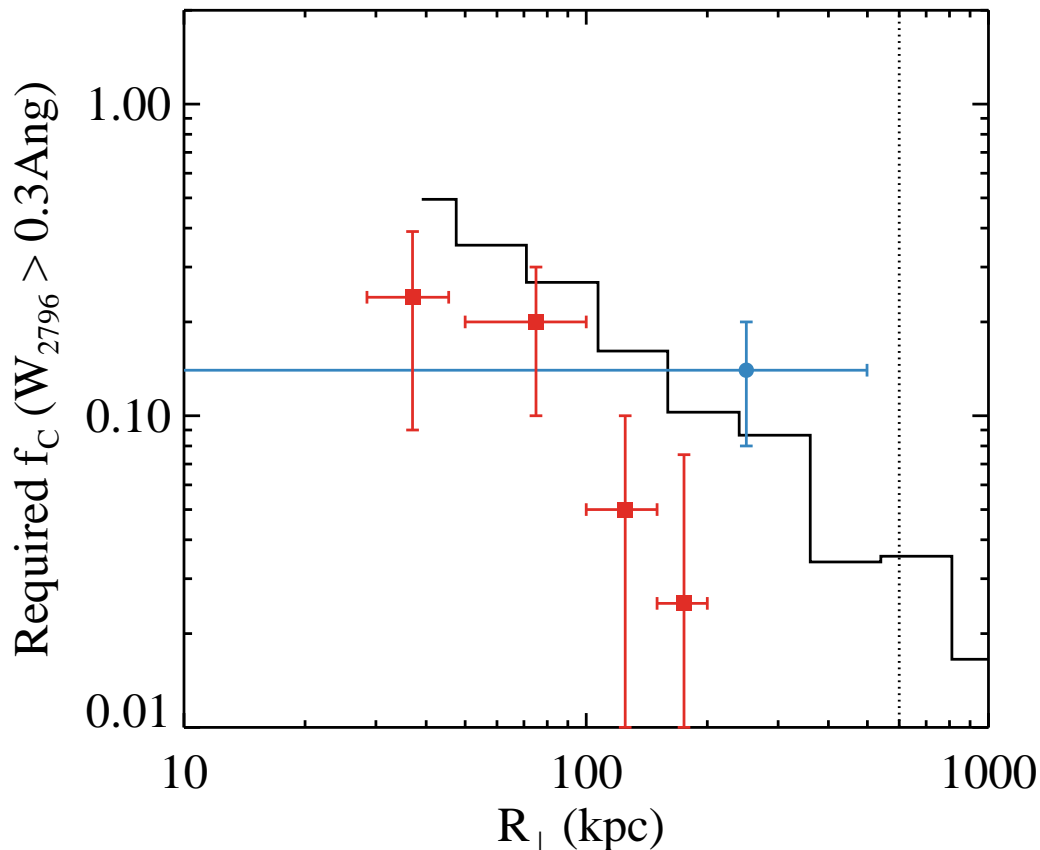


FIG. 18.— Estimated covering fraction  $f_c$  (black curve) required for strong Mg II absorption systems ( $W_{2796} > 0.3\text{\AA}$ ) to reproduce the average equivalent width observed in spectral stacks probing LRGs (Zhu et al. 2014). See the Appendix for a discussion of the methodology. The colored points show estimations of the covering fraction from (red Bowen & Chelouche 2011) and (blue Gauthier & Chen 2011).

present-day galaxies. At  $z \sim 0$ , surveys of 21cm emission<sup>24</sup> give a cosmological H I mass density  $\Omega_{\text{HI}} = 4.3 \times 10^{-4} h_{70}^{-1}$  (Zwaan et al. 2005a; Martin et al. 2010a). It is reasonable to assume that all of the Mg associated with this atomic gas<sup>25</sup> is  $\text{Mg}^+$ . Therefore, to estimate the mass density of  $\text{Mg}^+$  in the gas-phase, one must adopt a metallicity  $[\text{Mg}/\text{H}]$  and a dust depletion  $D_{\text{Mg}}$ . For the former, Zwaan et al. (2005b) estimate the ISM of the population of galaxies dominating  $\rho_{\text{HI}}$  to be  $\approx 1/2$  solar. For the latter, the Galactic ISM shows  $D_{\text{Mg}} \approx 0.3$  for all but the densest gas (Jenkins 2009). Combining these factors, we find

$$\rho(\text{Mg}^+)_{\text{ISM}} = \rho_c \Omega_{\text{HI}} \left( \frac{Mg}{H} \right) \left( \frac{m_{\text{Mg}}}{m_p} \right) D_{\text{Mg}} = 5.2 \times 10^{-8} \rho_c \quad (2)$$

We can compare this quantity to the dark matter density today,  $\rho_{\text{DM}} = \Omega_{\text{DM}} \rho_c$  with  $\Omega_{\text{DM}} = 0.22$ . This gives the ratio of  $\text{Mg}^+$  to dark matter of  $\rho(\text{Mg}^+)_{\text{ISM}}/\rho_{\text{DM}} = 2 \times 10^{-7}$ . This exceeds the Z14 estimates by over an order of magnitude. Even if we allow for a greater depletion factor (dense gas in the Galaxy exhibits  $D_{\text{Mg}} \lesssim 0.1$  Jenkins 2009), the gas in the ISM easily accounts for the Z14 results. In fact, we are forced to conclude that the Z14 measurements are biased low, perhaps due to dust obscuration (Ostriker & Heisler 1984) and/or a systematic underestimate of the column densities from their equivalent width measurements (i.e. line-saturation).

<sup>24</sup> Survey of the damped Ly $\alpha$  systems (DLAs) give even larger

values at  $z \approx 0.5$  (Rao et al. 2006; Prochaska & Wolfe 2009).

<sup>25</sup> There could be additional  $\text{Mg}^+$  in molecular gas.